ETH Library

Measurement of the inclusive t t ¯ cross section in pp collisions at √s=5.02 TeV using final states with at least one charged lepton

Journal Article

Author(s):
CMS Collaboration; Sirunyan, Albert M.; Bachmair, Felix; Bäni, Lukas; Berger, Pirmin; Bianchini, Lorenzo; Casal, Bruno; Dissertori, Günther; Dittmar, Michael; Donegà, Mauro; Grab, Christoph; Heidegger, Constantin; Hits, Dmitry; Hoss, Jan; Kasieczka, Gregor; Klijnsma, Thomas; Lustermann, Werner; Mangano, Boris; Marionneau, Matthieu; Meinhard, Maren T.; Meister, Daniel; Micheli, Francesco; Musella, Pasquale; Nessi-Tedaldi, Francesca; Pandolfi, Francesco; Pata, Joosep; Pauss, Felicitas; Perrin, Gaël; Perrozzi, Luca; Quittnat, Milena; Reichmann, Michael; Schönenberger, Myriam; Shchutska, Lesya; Tavolaro, Vittorio R.; Theofilatos, Konstantinos; Vesterbacka Olsson, Minna L.; Wallny, Rainer; Zhu, De Hua; et al.

Publication date:
2018-03

Permanent link:
https://doi.org/10.3929/ethz-b-000254398

Rights / license:
Creative Commons Attribution 4.0 International

Originally published in:
Journal of High Energy Physics 2018, https://doi.org/10.1007/JHEP03(2018)115

This page was generated automatically upon download from the ETH Zurich Research Collection.
For more information, please consult the Terms of use.

Published for SISSA by Springer

Received: *November 8, 2017*
Revised: *February 9, 2018*
Accepted: *March 5, 2018*
Published: *March 20, 2018*

Measurement of the inclusive $\mathrm{t\bar{t}}$ cross section in pp collisions at $\sqrt{s} = 5.02\,\mathrm{TeV}$ using final states with at least one charged lepton

The CMS collaboration

E-mail: cms-publication-committee-chair@cern.ch

Abstract: The top quark pair production cross section ($\sigma_{\mathrm{t\bar{t}}}$) is measured for the first time in pp collisions at a center-of-mass energy of 5.02 TeV. The data were collected by the CMS experiment at the LHC and correspond to an integrated luminosity of $27.4\,\mathrm{pb}^{-1}$. The measurement is performed by analyzing events with at least one charged lepton. The measured cross section is $\sigma_{\mathrm{t\bar{t}}} = 69.5 \pm 6.1\,(\mathrm{stat}) \pm 5.6\,(\mathrm{syst}) \pm 1.6\,(\mathrm{lumi})\,\mathrm{pb}$, with a total relative uncertainty of 12%. The result is in agreement with the expectation from the standard model. The impact of the presented measurement on the determination of the gluon distribution function is investigated.

Keywords: Hadron-Hadron scattering (experiments), Top physics

ArXiv ePrint: 1711.03143

Open Access, Copyright CERN,
for the benefit of the CMS Collaboration.
Article funded by SCOAP^3.

https://doi.org/10.1007/JHEP03(2018)115

JHEP03(2018)115

Contents

JHEP03(2018)115

1 Introduction

The top quark, the heaviest elementary particle in the standard model (SM), has been the subject of numerous detailed studies using hadron-hadron collisions. The pair production ($\mathrm{t\bar{t}}$) cross section ($\sigma_{\mathrm{t\bar{t}}}$) as a function of center-of-mass energy can be of interest for the extraction of the top quark pole mass [1] and has been used to constrain the gluon distribution function [2] at large fractions x of the proton longitudinal momentum carried by the gluon, where the gluon distribution is poorly known. Precise measurements of $\sigma_{\mathrm{t\bar{t}}}$ in proton-proton (pp) collisions have been published at $\sqrt{s}$ values of 7 and 8 [3–6] and 13 TeV [7–10] by the ATLAS and CMS Collaborations at the LHC.

In November 2015, the LHC delivered pp collisions at $\sqrt{s} = 5.02\,\mathrm{TeV}$. The fraction of $\mathrm{t\bar{t}}$ events initiated by gluon-gluon collisions grows monotonically with $\sqrt{s}$. It is around 73% at 5.02 TeV, as calculated with POWHEG (v2) [11–13] at next-to-leading order (NLO) using the NNPDF3.0 NLO [14] parton distribution functions (PDFs), and increases to around 86% at 13 TeV, making this new data set partially complementary to the higher-energy samples. Measurements of $\mathrm{t\bar{t}}$ production at various $\sqrt{s}$ probe different values of x and thus can provide complementary information on the gluon distribution. In addition, future measurements of $\sigma_{\mathrm{t\bar{t}}}$ in nuclear collisions at the same nucleon-nucleon center-of-mass energy [15, 16] would profit from the availability of a reference measurement in pp collisions at $\sqrt{s} = 5.02\,\mathrm{TeV}$, without the need to extrapolate from measurements at different $\sqrt{s}$. This has already been demonstrated with the first observation of the $\mathrm{t\bar{t}}$ process using proton-nucleus collisions at a higher nucleon-nucleon center-of-mass energy [17].

In the SM, top quarks in pp collisions are mostly produced as $\mathrm{t\bar{t}}$ pairs. Each top quark decays predominantly to a W boson and a bottom (b) quark. The $\mathrm{t\bar{t}}$ events are categorized according to the decay of the two W bosons. In $\mathrm{t\bar{t}}$ events where one W boson decays leptonically and the other hadronically (ℓ+jets channel), the final state presents a typical signature of one isolated lepton, missing transverse momentum, two jets from the W boson hadronic decay, and two jets coming from the hadronization of the b quarks ("b jets"). On the other hand, in $\mathrm{t\bar{t}}$ events where both W bosons decay leptonically (dilepton channel), the final state contains two leptons of opposite electric charge, missing transverse momentum, and at least two b jets. The ℓ+jets channel has a large branching ratio with a moderate amount of background, while the dilepton channel is characterized by a high purity.

This analysis represents the first measurement of $\sigma_{\mathrm{t\bar{t}}}$ in pp collisions at $\sqrt{s} = 5.02\,\mathrm{TeV}$ using $\mathrm{t\bar{t}}$ candidate events with ℓ+jets, where leptons are either electrons ($\ell = \mathrm{e}$) or muons ($\ell = \mu$), and dilepton ($\mathrm{e}^{\pm}\mu^{\mp}$ or $\mu^{\pm}\mu^{\mp}$) final states. In the former case, $\sigma_{\mathrm{t\bar{t}}}$ is extracted by a fit to the distribution of a kinematic variable for different categories of lepton flavor and jet multiplicity, while in the latter an event counting approach is used. The two results are then combined in the final measurement, which is used as input to a quantum chromodynamics (QCD) analysis at next-to-next-to-leading order (NNLO) to investigate the impact on the determination of the gluon distribution in the less-explored kinematic range of $x \gtrsim 0.1$.

This paper is structured as follows. Section 2 describes the CMS detector. Section 3 gives a summary of the data and simulated samples used. After the discussion of the object reconstruction in section 4, and of the trigger and event selection in section 5, section 6 describes the determination of the background sources. The systematic uncertainties are discussed in section 7. The extraction of $\sigma_{\mathrm{t\bar{t}}}$ is presented in section 8 and the impact of the presented measurement on the determination of the proton PDFs is discussed in section 9. A summary of all the results is given in section 10.

2 The CMS detector

The central feature of the CMS apparatus is a superconducting solenoid of 6 m internal diameter, providing a magnetic field of 3.8 T parallel to the beam direction.

Within the solenoid volume are a silicon pixel and strip tracker, a lead tungstate crystal electromagnetic calorimeter (ECAL), and a brass and scintillator hadron calorimeter (HCAL), each composed of a barrel and two endcap sections. A preshower detector, consisting of two planes of silicon sensors interleaved with about 3 radiation lengths of lead, is located in front of the endcap regions of ECAL. Hadron forward calorimeters using steel as an absorber and quartz fibers as the sensitive material extend the pseudorapidity coverage provided by the barrel and endcap detectors from $|\eta| = 3.0$ to 5.2.

Charged particle trajectories with $|\eta| < 2.5$ are measured by the tracker system, while the energy deposits in ECAL and HCAL cells are summed to define the calorimeter tower energies, subsequently used to calculate the energies and directions of hadronic jets. Muons are detected in the pseudorapidity window $|\eta| < 2.4$ in gas-ionization detectors embedded in the steel flux-return yoke outside the solenoid. Photons and electrons are reconstructed by their deposited energy in groups of ECAL crystals ("clusters"). Events of interest are selected using a two-tiered trigger system [18]. The first level, composed of custom hardware processors, uses information from the calorimeters and muon detectors to select events at a rate of around 100 kHz within a time interval of less than 4 μs. The second level, known as the high-level trigger, consists of a farm of processors running a version of the full event reconstruction software optimized for fast processing, and reduces the event rate to around 1 kHz before data storage.

A more detailed description of the CMS detector, together with a definition of the coordinate system used and the relevant kinematic variables, can be found in ref. [19].

3 Data, simulated samples and theoretical cross section

This analysis is based on an integrated luminosity of $27.4 \pm 0.6\,\mathrm{pb}^{-1}$ [20]. The presence of multiple proton collisions in the same or nearby bunch crossings ("pileup") results in an average number of overlapping interactions estimated online to be 1.4, assuming a total inelastic cross section of 65 mb.

Several Monte Carlo (MC) event generators are used to simulate signal and background events. The NLO POWHEG (v2) [11–13] generator is used for $\mathrm{t\bar{t}}$ events, assuming a value of 172.5 GeV for the top quark mass (m_{top}). These events are passed to PYTHIA (v8.205) [21, 22] to simulate parton showering, hadronization, and the underlying event, using the CUETP8M1 [23, 24] tune for the default $\mathrm{t\bar{t}}$ MC sample. The NNPDF3.0 NLO PDFs with strong coupling $\alpha_{\mathrm{s}}(M_{\mathrm{Z}}) = 0.118$ at the Z boson mass scale M_{Z} are utilized in the MC calculations.

The MadGraph5_aMC@NLO (v5_2.2.2) generator [25] is used to simulate W boson production with additional jets (W+jets), and high-mass (>50 GeV) Drell-Yan quark-antiquark annihilation into lepton-antilepton pairs through Z boson or virtual-photon exchange (referred to as "Z/γ^*"). The simulation includes up to two extra partons at matrix element level, and the FxFx merging procedure [26] is used to interface with PYTHIA. Low-mass Z/γ^* events (20–50 GeV) are simulated with PYTHIA. The normalization of the W+jets and Z/γ^* processes is either derived from data (in the dilepton channel) or estimated based on the NNLO cross sections (in the ℓ+jets channel) from the FEWZ program (v3.1.b2) [27]. Single top quark plus W boson events (tW) are simulated using POWHEG (v1) [28, 29] interfaced with PYTHIA, and are normalized to the approximate NNLO cross sections [30]. The contributions from WW and WZ production (referred to as

"WV") are simulated with PYTHIA, and are normalized to the NLO cross sections calculated with the MCFM (v8.0) program [31]. All generated events undergo a full GEANT4 [32] simulation of the detector response.

The expected signal yields are normalized to the value of the SM prediction for the $\mathrm{t\bar{t}}$ production cross section:

$$\sigma^{\mathrm{NNLO}} = 68.9\ ^{+1.9}_{-2.3}\,(\mathrm{scale}) \pm 2.3\,(\mathrm{PDF})\ ^{+1.4}_{-1.0}\ (\alpha_{\mathrm{s}})\,\mathrm{pb}, \tag{3.1}$$

as calculated with the TOP++ program [33] at NNLO in perturbative QCD, including soft-gluon resummation at next-to-next-to-leading-logarithmic order [34], using the NNPDF 3.0 NNLO PDF set, with $\alpha_{\mathrm{s}}(M_{\mathrm{Z}}) = 0.118$ and $m_{\mathrm{top}} = 172.5\,\mathrm{GeV}$. The systematic uncertainties in the theoretical $\mathrm{t\bar{t}}$ cross section are associated with the choice of the renormalization (μ_{R}) and factorization (μ_{F}) scales — nominally set at $\mu_{\mathrm{R}} = \mu_{\mathrm{F}} = \sqrt{m^2_{\mathrm{top}} + p^2_{\mathrm{T,top}}}$ with $p_{\mathrm{T,top}}$ the top quark transverse momentum — as well as with the PDF set and the α_s value. The uncertainty of 0.1% in the LHC beam energy [35] translates into an additional uncertainty of 0.22 pb in the expected cross section, with negligible impact on the acceptance of any of the channels included in this analysis.

4 Object reconstruction

The particle-flow (PF) algorithm [36] is used to reconstruct and identify individual particles using an optimized combination of information from the various elements of the CMS detector.

The electron momentum is calculated by combining the energy measurement in the ECAL with the momentum measurement in the tracker, taking into account the bremsstrahlung photons spatially compatible with originating from the electron track. The momentum resolution for electrons with transverse momentum $p_{\mathrm{T}} \approx 45\,\mathrm{GeV}$ from $\mathrm{Z} \to \mathrm{ee}$ decays ranges from 1.7% for nonshowering electrons in the barrel region to 4.5% for showering electrons in the endcaps [37]. Muon candidates are reconstructed from a combination of the information collected by the muon spectrometer and the silicon tracker. This results in a relative p_{T} resolution of 1.3–2.0% in the barrel and better than 6% in the endcaps, for muons with $20 < p_{\mathrm{T}} < 100\,\mathrm{GeV}$ and within the range $|\eta| < 2.4$ [38, 39]. The photon energy is directly obtained from the ECAL measurement, corrected for zero-suppression effects. The charged hadron energies are determined from a combination of their momenta measured in the tracker and the matching ECAL and HCAL energy deposits, corrected for zero-suppression effects and for the response function of the calorimeters to hadronic showers. Finally, the neutral hadron energies are obtained from the corresponding corrected ECAL and HCAL energies.

The missing transverse momentum vector is defined as the negative vector sum of the momenta of all reconstructed PF candidates in an event, projected onto the plane perpendicular to the direction of the proton beams. Its magnitude is referred to as $p_{\mathrm{T}}^{\mathrm{miss}}$ and the corrections to jet momenta are propagated to the $p_{\mathrm{T}}^{\mathrm{miss}}$ calculation [40].

The reconstructed vertex with the largest value of summed physics-object p_{T}^2 is taken to be the primary pp interaction vertex. The physics objects are the jets, clustered using the jet finding algorithm [41, 42] with the tracks assigned to the vertex as inputs, and the associated $p_{\mathrm{T}}^{\mathrm{miss}}$. The isolation of electron and muon candidates from nearby jet activity is then evaluated as follows. For electron and muon candidates, a cone of $\Delta R = 0.3$ and 0.4, respectively, is constructed around the direction of the lepton track at the primary event vertex, where ΔR is defined as $\sqrt{(\Delta\eta)^2 + (\Delta\phi)^2}$, and $\Delta\eta$ and $\Delta\phi$ are the differences in pseudorapidity and azimuthal angle between the directions of the lepton and another particle. A relative isolation discriminant, I_{rel}, is calculated by the ratio between the scalar p_{T} sum of all particle candidates inside the cone consistent with originating from the primary vertex and the p_{T} of the lepton candidate. In this sum, we exclude the p_{T} of the lepton candidate. The neutral particle contribution to I_{rel} is corrected for energy deposits from pileup interactions using different techniques for electrons and muons. For muons, half of the total p_{T} of the charged hadron PF candidates not originating from the primary vertex is subtracted. The factor of one half accounts for the different fraction of charged and neutral particles in the cone. For electrons, the FastJet technique [43] is used, in which the median of the energy-density distribution of neutral particles (within the area of any jet in the event) multiplied by the geometric area of the isolation cone — scaled by a factor that accounts for the residual η-dependence of the average energy deposition due to pileup — is subtracted.

The efficiency of the lepton selection is measured using a “tag-and-probe” method in same-flavor dilepton events enriched in Z boson candidates, following the method of ref. [44]. The sample of $\mathrm{Z} \to \mu^+\mu^-$ events used for muon efficiency extraction is selected by the same trigger requirement used by the main analysis (section 5). The $\mathrm{Z} \to \mathrm{e}^+\mathrm{e}^-$ sample for electron efficiency extraction makes use of events that satisfy a diphoton trigger with symmetric transverse energy, $E_{\mathrm{T}} = \sum_i E_i \sin\theta_i$, thresholds of $E_{\mathrm{T}} = 15\,\mathrm{GeV}$ covering the full tracker acceptance, where E_i is the energy seen by the calorimeters for the ith particle, θ_i is the polar angle of particle i, and the sum is over all particles emitted into a fixed solid angle in the event. Pairs of photon candidates above the E_{T} threshold are accepted only if their invariant mass is above 50 GeV. The trigger selection requires a loose identification using cluster shower shapes and a selection based on the ratio of the hadronic to the electromagnetic energy of the photon candidates. Based on a comparison of the lepton selection efficiency in data and simulation, the event yield in simulation is corrected using data-to-simulation scale factors.

Jets are reconstructed from the PF candidates using the anti-k_{T} clustering algorithm [41] with a distance parameter of 0.4. Jets closer than $\Delta R = 0.3$ to the nearest muon or electron are discarded. Jet energy corrections extracted from full detector simulation are also applied as a function of jet p_{T} and η [45] to data and simulation. A residual correction to the data is applied to account for the discrepancy between data and simulation in the jet response.

5 Event selection

The event sample is selected by a loose online trigger and further filtered offline to remove noncollision events, such as beam-gas interactions or cosmic rays. Collision events containing one high-p_{T} electron (muon) candidate are selected online by requiring values of E_{T}

JHEP03(2018)115

(p_{T}) greater than 40 (15) GeV and of $|\eta|$ less than 3.1 (2.5). The measured trigger efficiency for each decay channel, relative to the final selection, is higher than 90%.

In the ℓ+jets analysis, electron candidates are selected if they have $p_{\mathrm{T}} > 40\,\mathrm{GeV}$ and $|\eta| < 2.1$. Further identification and isolation criteria are applied to the electron candidates. Electrons reconstructed in the ECAL barrel (endcap) are required to have $I_{\mathrm{rel}} < 4$ (5)%. Electron candidates in the $1.44 < |\eta| < 1.57$ region, i.e., in the transition region between the barrel and endcap sections of the ECAL, are excluded because the reconstruction of an electron object in this region is less efficient. Muons are required to have $p_{\mathrm{T}} > 25\,\mathrm{GeV}$ and $|\eta| < 2.1$. Additional identification criteria are applied and I_{rel} is required to be $< 15\%$. Events are rejected if they contain extra electrons or muons identified using a looser set of identification criteria and have $p_{\mathrm{T}} > 10$ or $15\,\mathrm{GeV}$, respectively.

The distinct signature of two b jets, expected in $\mathrm{t\bar{t}}$ decays, is rare in background events, and thus is exploited in the ℓ+jets analysis. Backgrounds from W+jets, QCD multijet, and Z/γ^* events are controlled by counting the number of b jets in the selected events. In addition, two light-flavor jets are expected to be produced in the decay of one of the W bosons for signal events. The correlation in phase space of these light jets carries a distinctive hallmark with respect to the main backgrounds. To that end, jets are selected if they have $p_{\mathrm{T}} > 30\,\mathrm{GeV}$ and $|\eta| < 2.4$. The flavor of the jets is identified using a combined secondary vertex algorithm [46] with an operating point that yields a b jet identification efficiency of about 70%, and misidentification (mistag) probabilities of about 1% and 15% for light-flavor (u, d, s, and gluons) and c jets, respectively. The event selection requires at least two non-b-tagged jets to be identified as candidates from the W boson hadronic decay. Additional jets passing the b quark identification criteria are counted and used to classify the selected events in none (0 b), exactly one (1 b), or at least two ($\geq$2 b) tagged jet categories. The efficiency of the b jet identification algorithm is measured *in situ*, simultaneously with the signal cross section.

Dilepton events are required to contain at least one muon candidate at trigger level. No requirement on the presence of electron candidates is made at trigger level owing to the relatively high-E_{T} threshold (40 GeV) of the trigger. Electrons are selected if they have $p_{\mathrm{T}} > 20\,\mathrm{GeV}$, $|\eta| < 2.4$, and $I_{\mathrm{rel}} < 9$ (or 12)% if in the barrel (or one of the endcaps). As in the ℓ+jets channel, electrons detected in the transition region between the barrel and endcap sections of the ECAL are excluded. Muons are required to have $p_{\mathrm{T}} > 18\,\mathrm{GeV}$, $|\eta| < 2.1$, and $I_{\mathrm{rel}} < 15\%$. At least two jets satisfying the criteria $p_{\mathrm{T}} > 25\,\mathrm{GeV}$ and $|\eta| < 3$ are required. Events are subsequently selected if they have a pair of leptons with opposite charge ($\mathrm{e}^{\pm}\mu^{\mp}$ or $\mu^{\pm}\mu^{\mp}$) passing the requirements listed above. In events with more than one pair of leptons passing the above selection, the two leptons of opposite charge that yield the highest scalar p_{T} sum are selected.

Candidate events with dilepton invariant masses of $M_{\ell\ell} < 20\,\mathrm{GeV}$ are removed to suppress events from decays of heavy-flavor resonances and low-mass Z/γ^* processes. Dilepton events with two muons in the final state are still dominated by the Z/γ^* background. In order to suppress this contribution, events in the Z boson mass window of $76 < M_{\ell\ell} < 106\,\mathrm{GeV}$ are vetoed in this channel. To further suppress the Z/γ^* events, a requirement on $p_{\mathrm{T}}^{\mathrm{miss}}$ of $>$35 GeV is imposed.

In both the ℓ+jets and dilepton analyses, events with τ leptons are considered as signal if they decay to electrons or muons that satisfy the selection requirements, and are included in the simulation.

6 Background estimation

6.1 The ℓ+jets final state

In the ℓ+jets analysis, the contributions of all background processes are estimated from simulation, with the exception of the QCD multijet background. Due to its large cross section, there is a nonnegligible contribution from the latter faking a $\mathrm{t\bar{t}}$ event with ℓ+jets in the final state. Both the contribution from hard fragmentation of c and b quarks whose hadrons decay semileptonically, and the contribution from misidentified leptons, such as from either punch-through hadrons or collimated jets with a high electromagnetic fraction, can yield ℓ+jets-like topologies.

The estimation of the QCD multijet background is separately performed for the events with 0, 1, or $\geq$2 b jets using a control region where either the muon candidate fails a looser isolation requirement ($I_{\mathrm{rel}} < 20\%$) or the electron candidate fails the identification criteria. The choice of the QCD multijet control region has been made in such a way as to minimize the contamination due to the signal and W+jets events, while retaining a large number of events in the sample for the estimation of this type of background. The initial normalization of the QCD multijet contribution in the signal region is derived from events with $p_{\mathrm{T}}^{\mathrm{miss}} < 20\,\mathrm{GeV}$ ("reduced-signal" region). Events in both the reduced-signal and control regions fulfilling this requirement are counted. After subtracting the expected contributions from non-QCD processes, the ratio between the numbers of events observed in the reduced-signal region and in the control region, is used as a transfer factor to normalize the QCD multijet background estimate. In both the electron and muon channels, a 30% uncertainty is assigned to the estimate of the expected contribution from non-QCD processes, estimated after varying the QCD scales in the W+jets simulation. This uncertainty propagates as both a normalization and a shape uncertainty in the predicted distributions for the QCD multijet processes. The variations are applied independently in the reduced-signal and control regions in order to determine an uncertainty envelope. A more accurate normalization for this contribution is obtained by the fit performed to extract the final cross section, described in section 8.1.

6.2 The dilepton final state

Final states with two genuine leptons can originate from background processes, primarily from $\mathrm{Z}/\gamma^* \to \tau^+\tau^-$ (where the τ leptonic decays can yield $\mathrm{e}^{\pm}\mu^{\mp}$ or $\mu^{\pm}\mu^{\mp}$ plus $p_{\mathrm{T}}^{\mathrm{miss}}$ due to the neutrinos), tW, and WV events. Other background sources, such as W+jets events or $\mathrm{t\bar{t}}$ production in the ℓ+jets final state, can contaminate the signal sample if a jet is misidentified as a lepton, or if an event contains a lepton from the decay of b or c hadrons. These are included in the "non-W/Z" category, since genuine leptons are defined as originating from decays of W or Z bosons. The yields from tW and WV events are estimated from simulation, while the contribution of the Z/γ^* background is evaluated using control samples in data. The rate of non-W/Z backgrounds is extracted from control samples in data for the $e^\pm\mu^\mp$ channel and is estimated from simulation for the $\mu^\pm\mu^\mp$ channel.

A scale factor for the Z/γ^* background normalization is estimated, as in ref. [47], from the number of events within the Z boson mass window in data, which is extrapolated to the number of events outside the window. A scale factor of $0.91 \pm 0.14\,(\text{stat})$ is obtained in the $e^\pm\mu^\mp$ channel, and $0.96 \pm 0.78\,(\text{stat})$ in the $\mu^\pm\mu^\mp$ channel. The estimation is performed using events with at least two jets, and the dependence on different jet multiplicities is discussed in section 7.

The non-W/Z background in the $e^\pm\mu^\mp$ channel is estimated using an extrapolation from a control region of same-sign (SS) dilepton events to the signal region of opposite-sign (OS) dileptons. The SS control region is defined using the same criteria as for the nominal signal region, except requiring dilepton pairs of the same charge. The muon isolation requirement is relaxed in order to enhance the number of events. The SS dilepton events predominantly contain at least one misidentified lepton. Other SM processes produce genuine SS or charge-misidentified dilepton events with significantly smaller rates; these are estimated using simulation and subtracted from the observed number of events in data. The scaling from the SS control region in data to the signal region is performed using an extrapolation factor extracted from MC simulation, given by the ratio of the number of OS events with misidentified leptons to the number of SS events with misidentified leptons. The resulting estimate for the non-W/Z background is $1.0 \pm 0.9\,(\text{stat})$ events, where the central value comes from the estimation using events with at least two jets. No particular dependence of this scale factor is observed for different jet multiplicities within the large statistical uncertainty.

7 Systematic uncertainties

The integrated luminosity has been estimated offline using a pixel cluster counting method [20]. The estimation takes into account normalization uncertainties and uncertainties related to the different conditions during typical physics periods relative to the specially tailored beam-separation scans, adding up to a total uncertainty of ±2.3%.

The uncertainties in the electron trigger efficiency (1.5%) and the identification and isolation efficiency (2.5%) are estimated by changing the values of the data-to-simulation scale factors within their uncertainties, as obtained from the "tag-and-probe" method. The uncertainty in the muon identification and isolation efficiency, including the trigger efficiency, is 3% and covers one standard deviation of the scale factor from unity.

The impact of the uncertainty in the jet energy scale (JES) is estimated by changing the p_T- and η-dependent JES corrections by a constant 2.8% [45, 48]. The uncertainty in jet energy resolution (JER) is estimated through η-dependent changes in the JER corrections to the simulation [45, 48]. The uncertainty arising from the use of p_T^{miss} in the $\mu^\pm\mu^\mp$ channel is dominated by the unclustered energy contribution to p_T^{miss} [40]. Finally, a 30% uncertainty is conservatively assigned to the jet misidentification probability in the

JHEP03(2018)115

ℓ+jets analysis, as no dedicated measurement of this quantity has been performed for the considered data set.

Theoretical uncertainties in the simulation of $\mathrm{t\bar{t}}$ production cause a systematic bias related to the missing higher-order diagrams in POWHEG, which is estimated through studies of the signal modeling by modifying the $\mu_{\mathrm{R}}, \mu_{\mathrm{F}}$ scales within a factor of two with respect to their nominal value. In the ℓ+jets analysis, the impact of the $\mu_{\mathrm{R}}, \mu_{\mathrm{F}}$ variations are examined independently, while in the dilepton analysis they are varied simultaneously. In both analyses, these variations are applied independently at the matrix element (ME) and parton shower (PS) levels. The uncertainty arising from the hadronization model mainly affects the JES and the fragmentation of jets. The hadronization uncertainty is determined by comparing samples of events generated with POWHEG, where the hadronization is either modeled with PYTHIA or HERWIG++ (v2.7.1) [49]. This also accounts for differences in the PS model and the underlying event. The uncertainty from the choice of PDF is determined by reweighting the sample of simulated $\mathrm{t\bar{t}}$ events according to the root-mean-square (RMS) variation of the NNPDF3.0 replica set. Two extra variations of α_{s} are added in quadrature to determine the total PDF uncertainty.

In the ℓ+jets analysis, the uncertainty in the choice of the $\mu_{\mathrm{R}}, \mu_{\mathrm{F}}$ scales in the W+jets simulation is taken into account by considering alternative shapes and yields after varying independently the $\mu_{\mathrm{R}}, \mu_{\mathrm{F}}$ scales, following a similar procedure to that described above for the signal. Due to the finite event count in the W+jets simulated sample, an additional bin-by-bin uncertainty is assigned by generating an alternative shape to fit (see section 8.1), where the bin prediction is varied by ±1 standard deviation, while keeping all the other bins at their nominal expectation. The uncertainty assigned to the QCD multijet background includes the statistical uncertainty in the data, and the uncertainty from the non-QCD multijet contributions subtracted from the control region, as described in section 6.1, and an additional 30%–100% normalization uncertainty. The latter depends on the event category and stems from the measured difference with respect to an alternative estimate of the QCD normalization based on the transverse mass, m_{T}, of the lepton and $p_{\mathrm{T}}^{\mathrm{miss}}$ system. The magnitude of m_{T} equals $\sqrt{2 p_{\mathrm{T}} p_{\mathrm{T}}^{\mathrm{miss}} (1 - \cos \Delta\phi)}$, where p_{T} is the lepton transverse momentum and $\Delta\phi$ is the azimuthal angle between the lepton and the direction of $\vec{p}_{\mathrm{T}}^{\mathrm{miss}}$. Finally, a 30% normalization uncertainty in the theoretical tW, Z/γ^{*}, and WV background cross sections is assigned [5], given the previously unexplored $\sqrt{s}$ value and that the final states contain several jets.

In the dilepton channel, an uncertainty of 30% is assumed [5] for the cross sections of the tW and WV backgrounds to cover the theoretical uncertainties and the effect of finite simulated samples. The uncertainty in the Z/γ^{*} estimation is calculated by combining in quadrature the statistical uncertainty and an additional 30% from the variation of the scale factor in the different levels of selection, resulting in uncertainties of about 30 and 80% in the $\mathrm{e}^{\pm}\mu^{\mp}$ and $\mu^{\pm}\mu^{\mp}$ channels, respectively. The systematic uncertainty in the non-W/Z background is estimated to be 90% in the $\mathrm{e}^{\pm}\mu^{\mp}$ channel and is dominated by the statistical uncertainty in the method. Owing to the limited sample size in the data, the method cannot be applied in the $\mu^{\pm}\mu^{\mp}$ channel. The estimation is therefore based on MC simulation, and an uncertainty of 100% is conservatively assigned.

8 Measurement of the $\mathrm{t\bar{t}}$ cross section

8.1 The ℓ+jets final state

In the ℓ+jets analysis, the $\mathrm{t\bar{t}}$ cross section is measured in a fiducial phase space by means of a fit. Two variables were independently considered for the fit, which are sensitive to the resonant behavior of the light jets produced from the W boson hadronic decay in a $\mathrm{t\bar{t}}$ event. Given that these light jets, here denoted by j and j', are correlated during production, they are also expected to be closer in phase space when compared to pairs of other jets in the event. The angular distance ΔR can thus be used as a metric to rank all pairs of non-b-tagged jets in the event, maximizing the probability of selecting those from the W boson hadronic decay in cases where more than two non-b-tagged jets are found. From simulation we expect that the signal peaks at low ΔR, while the background is uniformly distributed up to $\Delta R \approx 3$. Above that value, fewer events are expected and background processes are predicted to dominate. The invariant mass $M(j,j')$ of jets j and j' also has a distinctive peaking feature for the signal in contrast with a smooth background continuum. From simulation we expect that the minimum angular distance ΔR between all pairs of jets j and j', $\Delta R_{\min}(j,j')$, is robust against signal modeling uncertainties such as the choice of the $\mu_{\mathrm{R}}, \mu_{\mathrm{F}}$ scales and jet energy scale and resolution, while the $M(j,j')$ variable tends to be more affected by such uncertainties. Owing to its more robust systematic uncertainties and signal-to-background discrimination power, the $\Delta R_{\min}(j,j')$ variable is used to extract the $\mathrm{t\bar{t}}$ cross section.

In order to maximize the sensitivity of the analysis, the $\Delta R_{\min}(j,j')$ distributions are categorized according to the number of jets — in addition to the ones assigned to the W boson hadronic decay — passing the b quark identification criteria. In total, 6 categories are used, corresponding to electron or muon events with 0, 1, or $\geq$2 b jets. The expected number of signal and background events in each category prior to the fit and the observed yields are given in table 1. Good agreement is observed between data and expectations.

The $M(j,j')$ and $\Delta R_{\min}(j,j')$ distributions are shown in figure 1. The distributions have been combined for the e+jets and μ+jets channels to maximize the statistical precision and are shown for events with different b-tagged jet multiplicities. Fair agreement is observed between data and the pre-fit expectations.

A profile likelihood ratio (PLR) method, similar to the one employed in ref. [10], is used to perform the fit. In addition, a scale factor for the b tagging efficiency ($\mathrm{SF_b}$) is included as a parameter of interest in the fit. The PLR is written as:

$$\lambda(\mu, \mathrm{SF_b}) = \frac{\mathcal{L}(\mu, \mathrm{SF_b}, \hat{\hat{\Theta}})}{\mathcal{L}(\hat{\mu}, \hat{\mathrm{SF}}_{\mathrm{b}}, \hat{\Theta})}, \tag{8.1}$$

where $\mu = \sigma/\sigma_{\mathrm{theo}}$ is the signal strength (ratio of the observed $\mathrm{t\bar{t}}$ cross section to the expectation from theory) and Θ is a set of nuisance parameters that encode the effect on the expectations due to variations in the sources of the systematic uncertainties described in section 7. The quantities $\hat{\hat{\Theta}}$ correspond to the values of the nuisance parameters that maximize the likelihood for the specified signal strength and b tagging efficiency (conditional

Source	b tag category					
	0 b		1 b		≥2 b	
	e+jets	μ+jets	e+jets	μ+jets	e+jets	μ+jets
tW	3.03 ± 0.02	5.6 ± 0.03	2.49 ± 0.02	4.5 ± 0.03	0.39 ± 0.01	0.67 ± 0.01
W+jets	776 ± 17	1704 ± 26	13 ± 2	26 ± 3	0.2 ± 0.3	0.8 ± 0.6
Z/γ^*	136 ± 4	162 ± 5	1.7 ± 0.5	2.8 ± 0.6	0.1 ± 0.1	0.1 ± 0.1
WV	0.52 ± 0.01	1.01 ± 0.02	<0.01	<0.02	<0.01	<0.01
QCD multijet	440 ± 130	490 ± 150	3.6 ± 1.1	28 ± 8	2.5 ± 0.8	2.0 ± 0.8
$\mathrm{t\bar{t}}$ signal	22.8 ± 0.3	42.3 ± 0.4	36.9 ± 0.4	71.1 ± 0.5	13.8 ± 0.2	27.0 ± 0.3
Total	1380 ± 130	2410 ± 150	57.7 ± 2.4	131 ± 9	16.8 ± 0.9	31 ± 1
Observed data	1375	2406	61	129	19	33

Table 1. The number of expected background and signal events and the observed event yields in the different b tag categories for the e+jets and μ+jets analyses, prior to the fit. With the exception of the QCD multijet estimate, for which the total uncertainty is reported, the uncertainties reflect the statistical uncertainty in the simulated samples.

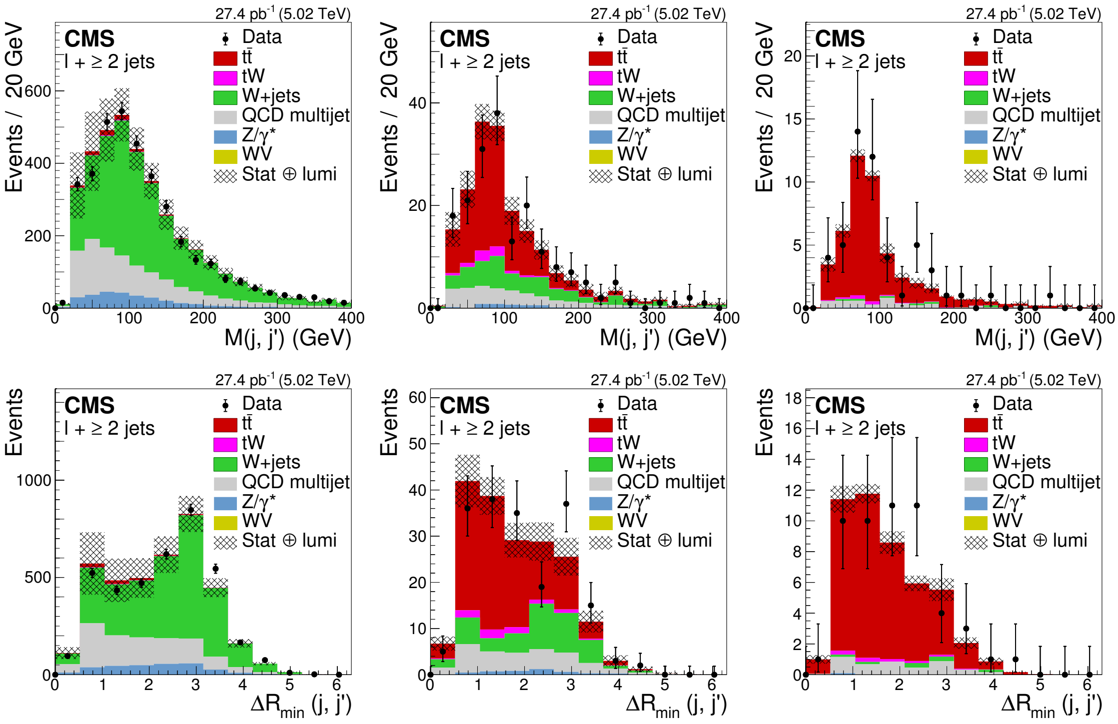

Figure 1. The predicted and observed distributions of the (upper row) $M(j,j')$ and (lower row) $\Delta R_{\min}(j,j')$ variable for ℓ+jets events in the 0 b (left), 1 b (center), and ≥2 b (right) tagged jet categories. The distributions from data are compared to the sum of the expectations for the signal and backgrounds prior to any fit. The QCD multijet background is estimated from data (see section 5.1). The cross-hatched band represents the statistical and the integrated luminosity uncertainties in the expected signal and background yields added in quadrature. The vertical bars on the data points represent the statistical uncertainties.

JHEP03(2018)115

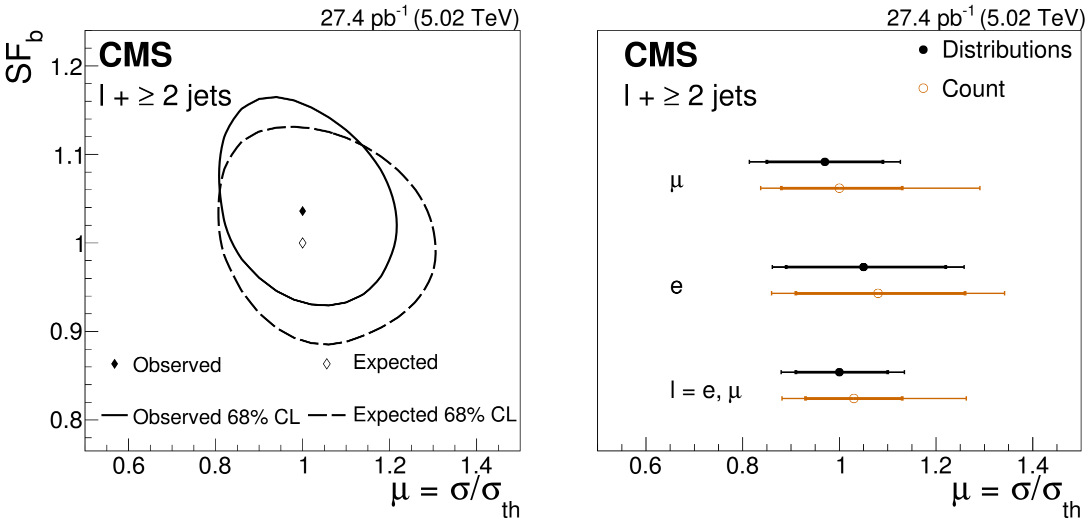

Figure 2. Left: the 68% CL contour obtained from the scan of the likelihood in ℓ+jets analysis, as a function of μ and $\mathrm{SF_b}$ in the ℓ+jets analysis. The solid (dashed) contour refers to the result from data (expectation from simulation). The solid (hollow) diamond represents the observed fit result (SM expectation). Right: summary of the signal strengths separately obtained in the e+jets and μ+jets channels, and after their combination in the ℓ+jets channel. The results of the analysis from the distributions are compared to those from the cross-check analysis with event counting (Count). The inner (outer) bars correspond to the statistical (total) uncertainty in the signal strengths.

likelihood), and $\hat{\mu}$, $\hat{\mathrm{SF}}_\mathrm{b}$, $\hat{\Theta}$ are, respectively, the values of the signal strength, b tagging efficiency, and nuisance parameters that maximize the likelihood.

Figure 2 (left) shows the two-dimensional contours at the 68% confidence level (CL) obtained from the scan of $-2\ln(\lambda)$, as functions of μ and $\mathrm{SF_b}$. The expected results, obtained using the Asimov data set [50], are compared to the observed results and found to be in agreement well within one standard deviation. The signal strength is obtained after profiling $\mathrm{SF_b}$ and the result is $\mu = 1.00\,^{+0.10}_{-0.09}\,(\mathrm{stat})\,^{+0.09}_{-0.08}\,(\mathrm{syst})$. As a cross-check, the signal strength is also extracted by fitting only the total number of events observed in each of the six categories. The observed value $\mu = 1.03\,^{+0.10}_{-0.10}\,(\mathrm{stat})\,^{+0.21}_{-0.11}\,(\mathrm{syst})$ is in agreement with the analysis using the $\Delta R_{\mathrm{min}}(j, j')$ distributions. Figure 2 (right) summarizes the results obtained for the signal strength fit in each channel separately from the analysis of the distributions and from event counting. In both cases, a large contribution to the uncertainty is systematic in nature, although the statistical component is still significant. In the ℓ+jets combination, the μ+jets channel is expected and observed to carry the largest weight.

In order to estimate the impact of the experimental systematic uncertainties in the measured signal strength, the fit is repeated after fixing one nuisance parameter at a time at its post-fit uncertainty (±1 standard deviation) values. The impact on the signal strength fit is then evaluated from the difference induced in the final result from this procedure. By repeating the fits, the effect of some nuisance parameters being fixed may be reabsorbed by a variation of the ones being profiled, owing to correlations. As such, the individual experimental uncertainties obtained and summarized in table 2 can only be interpreted as the observed post-fit values, and not as an absolute, orthogonalized breakdown of uncer-

Source	$\Delta\mu/\mu$	
	Distr.	Count
Statistical uncertainty	0.095	0.100
Experimental systematic uncertainty	0.085	0.160
Individual experimental uncertainties		
W+jets background	0.035	0.025
QCD multijet background	0.024	0.044
Other background	0.013	0.013
Jet energy scale	0.030	0.031
Jet energy resolution	0.006	0.023
b tagging	0.034	0.045
Electron efficiency	0.011	0.028
Muon efficiency	0.017	0.022
Theoretical uncertainties		
Hadronization model of $\mathrm{t\bar{t}}$ signal	0.028	0.069
$\mu_\mathrm{R}, \mu_\mathrm{F}$ scales of $\mathrm{t\bar{t}}$ signal (PS)	0.044	0.115
$\mu_\mathrm{R}, \mu_\mathrm{F}$ scales of $\mathrm{t\bar{t}}$ signal (ME)	<0.010	<0.010
Total uncertainty	0.127	0.189

Table 2. Estimated impact of each source of uncertainty in the value of μ extracted from the analysis of distributions, and in the cross-check from event counting. The "Other background" component includes the contributions from Z/γ^*, tW, and WV events. The total uncertainty is obtained by adding in quadrature the statistical, experimental systematic, and theoretical uncertainties. The individual experimental uncertainties are obtained by repeating the fit after fixing one nuisance parameter at a time at its post-fit uncertainty (±1 standard deviation) value. The values quoted have been symmetrized.

tainties. With respect to the event counting, the analysis of the distributions is less prone to the uncertainties in the QCD multijet background, jet energy resolution, and signal modeling. In both cases, the signal modeling uncertainties and the b tagging efficiency are among the largest sources of uncertainty.

The fiducial cross section is measured in events with one electron (muon) in the range $p_\mathrm{T} > 35$ (25) GeV and $|\eta| < 2.1$ (including the transition region for electrons), and at least two jets with $p_\mathrm{T} > 25\,\mathrm{GeV}$ and $|\eta| < 2.4$. After multiplying the signal strength by the theoretical expectations (eq. (3.1)), we find

$$\sigma_\mathrm{fid} = 20.8 \pm 2.0\,(\mathrm{stat}) \pm 1.8\,(\mathrm{syst}) \pm 0.5\,(\mathrm{lumi})\,\mathrm{pb}.$$

The combined acceptance in the e+jets and μ+jets channels is estimated using the NLO POWHEG simulation to be $\mathcal{A} = 0.301 \pm 0.007$, with the uncertainty being dominated by the variation of the $\mu_\mathrm{R}, \mu_\mathrm{F}$ scales at ME and PS levels and the hadronization model used for the $\mathrm{t\bar{t}}$ signal. The uncertainty due to the PDFs is included but verified to be less important. Taking into account the acceptance of the analysis and its uncertainty, the inclusive $\mathrm{t\bar{t}}$ cross section is determined to be

$$\sigma_{\mathrm{t\bar{t}}} = 68.9 \pm 6.5\,(\mathrm{stat}) \pm 6.1\,(\mathrm{syst}) \pm 1.6\,(\mathrm{lumi})\,\mathrm{pb},$$

in agreement with the SM prediction and attaining a 13% total relative uncertainty.

8.2 The dilepton final state

In the dilepton analysis, the $\mathrm{t\bar{t}}$ cross section is extracted from an event counting measurement. Figure 3 shows the distributions of the jet multiplicity and the scalar p_{T} sum of all jets (H_{T}), for events passing the dilepton criteria in the $\mathrm{e}^{\pm}\mu^{\mp}$ channel. In addition, it displays the lepton-pair invariant mass and p_{T} distributions, after requiring at least two jets in the event in the $\mathrm{e}^{\pm}\mu^{\mp}$ channel. Figure 4 shows the $p_{\mathrm{T}}^{\mathrm{miss}}$ and the lepton-pair invariant mass distributions in the $\mu^{\pm}\mu^{\mp}$ channel for events passing the dilepton criteria, and the Z boson veto with the $p_{\mathrm{T}}^{\mathrm{miss}} > 35\,\mathrm{GeV}$ requirement, in the second case. The predicted distributions take into account the efficiency corrections described in section 5 and the background estimations discussed in section 6.2. Good agreement is observed between the data and predictions for both signal and background.

The fiducial $\mathrm{t\bar{t}}$ production cross section is measured by counting events in the visible phase space (defined by the same p_{T}, $|\eta|$, and multiplicity requirements for leptons and jets as described in section 5, but including the transition region for electrons) and is denoted by σ_{fid}. It is extrapolated to the full phase space in order to determine the inclusive $\mathrm{t\bar{t}}$ cross section using the expression

$$\sigma_{\mathrm{t\bar{t}}} = \frac{N - N_{\mathrm{B}}}{\varepsilon\,\mathcal{A}\,\mathcal{L}} = \frac{\sigma_{\mathrm{fid}}}{\mathcal{A}}, \tag{8.2}$$

where N is the total number of dilepton events observed in data, N_{B} the number of estimated background events, ε the selection efficiency, $\mathcal{A}$ the acceptance, and $\mathcal{L}$ the integrated luminosity. Table 3 gives the total number of events observed in data, together with the total number of signal and background events expected from simulation or estimated from data, after the full set of selection criteria. The total detector, trigger, and reconstruction efficiency is estimated from data to be $\varepsilon = 0.55 \pm 0.02$ (0.57 ± 0.04) in the $\mathrm{e}^{\pm}\mu^{\mp}$ $(\mu^{\pm}\mu^{\mp})$ channel. Using the definitions above, the yields from table 3, and the systematic uncertainties from table 4, the measured fiducial cross section for $\mathrm{t\bar{t}}$ production is

$$\sigma_{\mathrm{fid}} = 41 \pm 10\,(\mathrm{stat}) \pm 2\,(\mathrm{syst}) \pm 1\,(\mathrm{lumi})\,\mathrm{pb}$$

in the $\mathrm{e}^{\pm}\mu^{\mp}$ channel and

$$\sigma_{\mathrm{fid}} = 22 \pm 11\,(\mathrm{stat}) \pm 4\,(\mathrm{syst}) \pm 1\,(\mathrm{lumi})\,\mathrm{pb}$$

in the $\mu^{\pm}\mu^{\mp}$ channel.

The acceptance, as estimated from MC simulation, is found to be $\mathcal{A} = 0.53 \pm 0.01$ (0.37 ± 0.01) in the $\mathrm{e}^{\pm}\mu^{\mp}$ $(\mu^{\pm}\mu^{\mp})$ channel. The statistical uncertainty (from MC simulation) is included in the uncertainty in $\mathcal{A}$. By extrapolating to the full phase space, the inclusive $\mathrm{t\bar{t}}$ cross section is measured to be

$$\sigma_{\mathrm{t\bar{t}}} = 77 \pm 19\,(\mathrm{stat}) \pm 4\,(\mathrm{syst}) \pm 2\,(\mathrm{lumi})\,\mathrm{pb}$$

JHEP03(2018)115

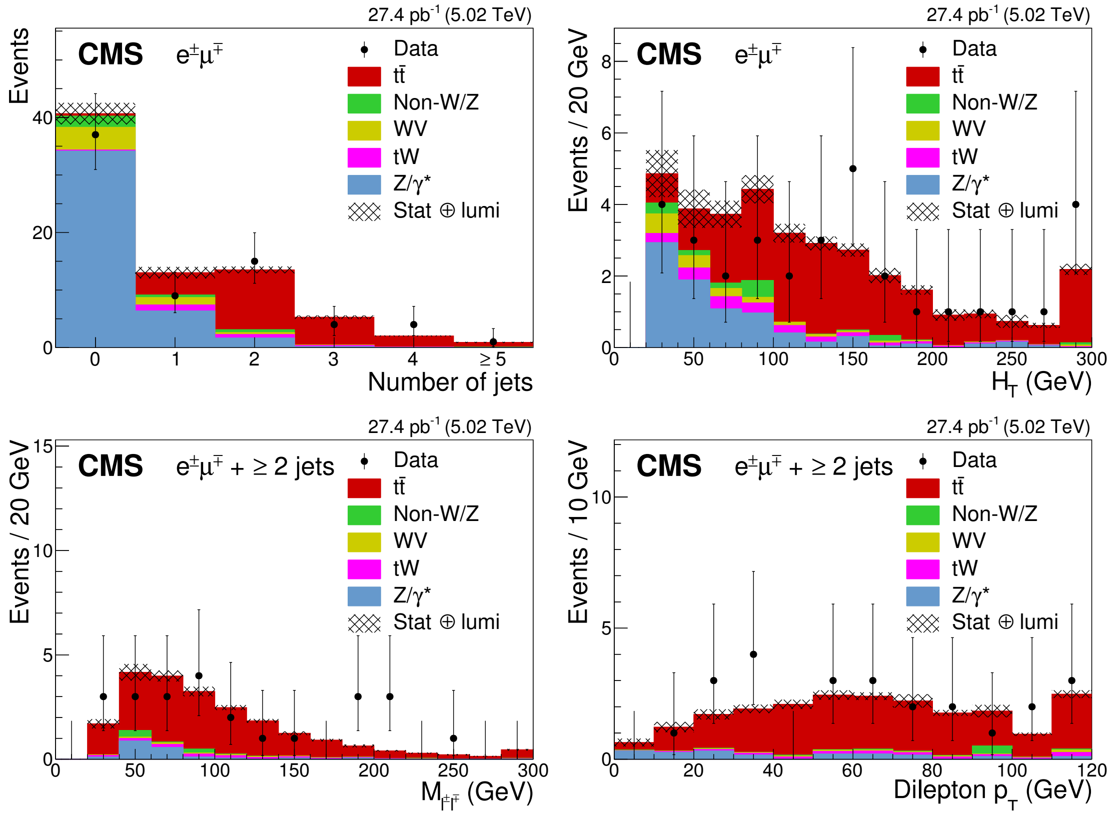

Figure 3. Predicted and observed distributions of the (upper row) jet multiplicity and scalar p_T sum of all jets (H_T) for events passing the dilepton criteria, and of the (lower row) invariant mass and p_T of the lepton pair after requiring at least two jets, in the $e^{\pm}\mu^{\mp}$ channel. The Z/γ^* and non-W/Z backgrounds are determined from data (see section 6.2). The cross-hatched band represents the statistical and integrated luminosity uncertainties in the expected signal and background yields added in quadrature. The vertical bars on the data points represent the statistical uncertainties. The last bin of the distributions contains the overflow events.

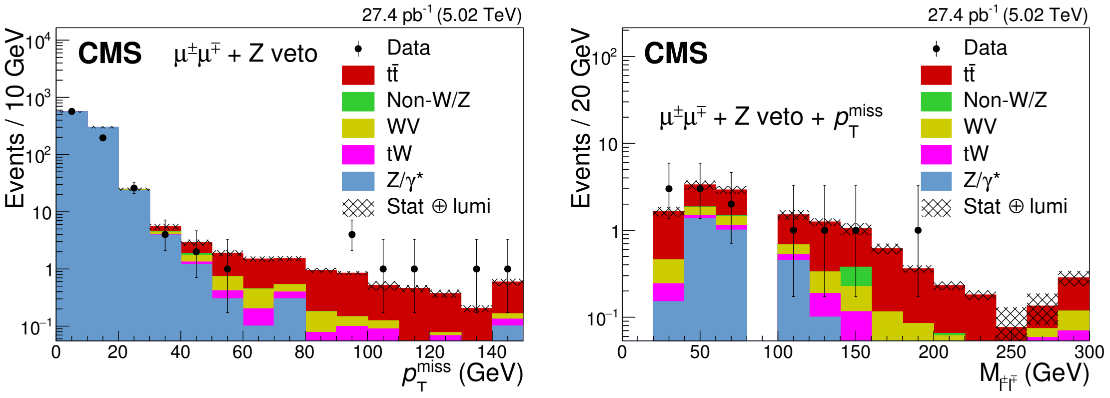

Figure 4. Predicted and observed distributions of the (left) p_T^{miss} in events passing the dilepton criteria and Z boson veto, and of the (right) invariant mass of the lepton pair after the $p_T^{miss} > 35\,\text{GeV}$ requirement in the $\mu^{\pm}\mu^{\mp}$ channel. The cross-hatched band represents the statistical and integrated luminosity uncertainties in the expected signal and background yields added in quadrature. The vertical bars on the data points represent the statistical uncertainties. The last bin of the distributions contains the overflow events.

Source	$e^{\pm}\mu^{\mp}$	$\mu^{\pm}\mu^{\mp}$
tW	0.92 ± 0.02	0.29 ± 0.01
Non-W/Z leptons	1.0 ± 0.9	0.04 ± 0.01
Z/γ^*	1.6 ± 0.2	1.1 ± 0.8
WV	0.44 ± 0.02	0.15 ± 0.01
$t\bar{t}$ signal	18.0 ± 0.3	6.4 ± 0.2
Total	22.0 ± 0.9	7.9 ± 0.8
Observed data	24	7

Table 3. The predicted and observed numbers of dilepton events obtained after applying the full selection. The values are given for the individual sources of background, $t\bar{t}$ signal, and data. The uncertainties correspond to the statistical component.

	$e^{\pm}\mu^{\mp}$		$\mu^{\pm}\mu^{\mp}$	
Source	$\Delta\sigma_{t\bar{t}}/\sigma_{t\bar{t}}$ (%)	$\Delta\sigma_{t\bar{t}}$ (pb)	$\Delta\sigma_{t\bar{t}}/\sigma_{t\bar{t}}$ (%)	$\Delta\sigma_{t\bar{t}}$ (pb)
Electron efficiency	1.4	1.0	—	—
Muon efficiency	3.0	2.3	6.1	3.6
Jet energy scale	1.3	1.0	1.3	0.7
Jet energy resolution	<0.1	<0.1	<0.1	<0.1
Missing transverse momentum	—	—	0.7	0.4
μ_R, μ_F scales of $t\bar{t}$ signal (PS)	1.2	0.9	1.7	1.0
μ_R, μ_F scales of $t\bar{t}$ signal (ME)	0.2	0.1	1.1	0.6
Hadronization model of $t\bar{t}$ signal	1.2	0.9	5.2	3.1
PDF	0.5	0.4	0.4	0.2
MC sample size	1.4	1.1	2.4	1.4
tW background	1.4	1.1	1.6	0.9
WV background	0.7	0.5	0.9	0.5
Z/γ^* background	2.7	2.1	15	9.1
Non-W/Z background	2.5	1.9	0.7	0.4
Total systematic uncertainty (w/o integrated luminosity)	5.8	4.4	18	11
Integrated luminosity	2.3	1.8	2.3	1.4
Statistical uncertainty	25	19	48	29
Total uncertainty	25	19	52	31

Table 4. Summary of the individual contributions to the systematic uncertainty in the $\sigma_{t\bar{t}}$ measurements for the dilepton channels. The relative uncertainties $\Delta\sigma_{t\bar{t}}/\sigma_{t\bar{t}}$ (in %), as well as absolute uncertainties in $\sigma_{t\bar{t}}$, $\Delta\sigma_{t\bar{t}}$ (in pb), are presented. The statistical and total uncertainties are also given, where the latter are the quadrature sum of the statistical and systematic uncertainties.

in the $\mathrm{e}^{\pm}\mu^{\mp}$ channel and

$$\sigma_{\mathrm{t\bar{t}}} = 59 \pm 29\,(\mathrm{stat}) \pm 11\,(\mathrm{syst}) \pm 1\,(\mathrm{lumi})\,\mathrm{pb}$$

in the $\mu^{\pm}\mu^{\mp}$ channel. Table 4 summarizes the relative and absolute statistical and systematic uncertainties from different sources contributing to $\sigma_{\mathrm{t\bar{t}}}$. The separate total systematic uncertainty without the uncertainty in the integrated luminosity, the part attributed to the integrated luminosity, and the statistical contribution are added in quadrature to obtain the total uncertainty. The cross sections, measured with a relative uncertainty of 25 and 52%, are in agreement with the SM prediction (eq. (3.1)) within the uncertainties in the measurements.

8.3 Combination

The three individual $\sigma_{\mathrm{t\bar{t}}}$ measurements are combined using the BLUE method [51, 52] to determine an overall $\mathrm{t\bar{t}}$ cross section. All systematic uncertainties are considered as fully correlated across all channels, with the following exceptions: the uncertainty associated with the finite event size of the simulated samples is taken as uncorrelated; the electron identification is not relevant for the $\mu\mu$ channel; and the b tagging and QCD multijet background uncertainties are only considered for the ℓ+jets channel. In the ℓ+jets channel, the WV and Z/γ^* backgrounds are not considered separately but as part of the "Other backgrounds" component, which is dominated by tW events. The uncertainty associated with this category is therefore treated as fully correlated with the tW uncertainty in the dileptonic channels and uncorrelated with the WV and Z/γ^* uncertainties.

The combined inclusive $\mathrm{t\bar{t}}$ cross section is measured to be:

$$\sigma_{\mathrm{t\bar{t}}} = 69.5 \pm 6.1\,(\mathrm{stat}) \pm 5.6\,(\mathrm{syst}) \pm 1.6\,(\mathrm{lumi})\,\mathrm{pb} = 69.5 \pm 8.4\,(\mathrm{total})\,\mathrm{pb},$$

where the total uncertainty is the sum in quadrature of the individual uncertainties. The weights of the individual measurements, to be understood in the sense of ref. [52], are 81.8% for ℓ+jets, 13.5% for $\mathrm{e}^{\pm}\mu^{\mp}$, and 4.7% for $\mu^{\pm}\mu^{\mp}$ channels.

The combined result is found to be robust by performing an iterative variant of the BLUE method [53] and varying some assumptions on the correlations of different combinations of systematic uncertainties. Also, the post-fit correlations between the nuisance parameters in the ℓ+jets channel have been checked and found to have negligible impact.

Figure 5 presents a summary of CMS measurements [5, 6, 9, 10] of $\sigma_{\mathrm{t\bar{t}}}$ in pp collisions at different $\sqrt{s}$ in the ℓ+jets and dilepton channels, compared to the NNLO+NNLL prediction using the NNPDF3.0 PDF set with $\alpha_{\mathrm{s}}(M_{\mathrm{Z}}) = 0.118$ and $m_{\mathrm{top}} = 172.5\,\mathrm{GeV}$. In the inset, the results from this analysis at $\sqrt{s} = 5.02\,\mathrm{TeV}$ are also compared to the predictions from the MMHT14 [54], CT14 [55], and ABMP16 [56] PDF sets, with the latter using $\alpha_{\mathrm{s}}(M_{\mathrm{Z}}) = 0.115$ and $m_{\mathrm{top}} = 170.4\,\mathrm{GeV}$. Theoretical predictions using different PDF sets have comparable values and uncertainties, once consistent values of α_{s} and m_{top} are associated with the respective PDF set.

JHEP03(2018)115

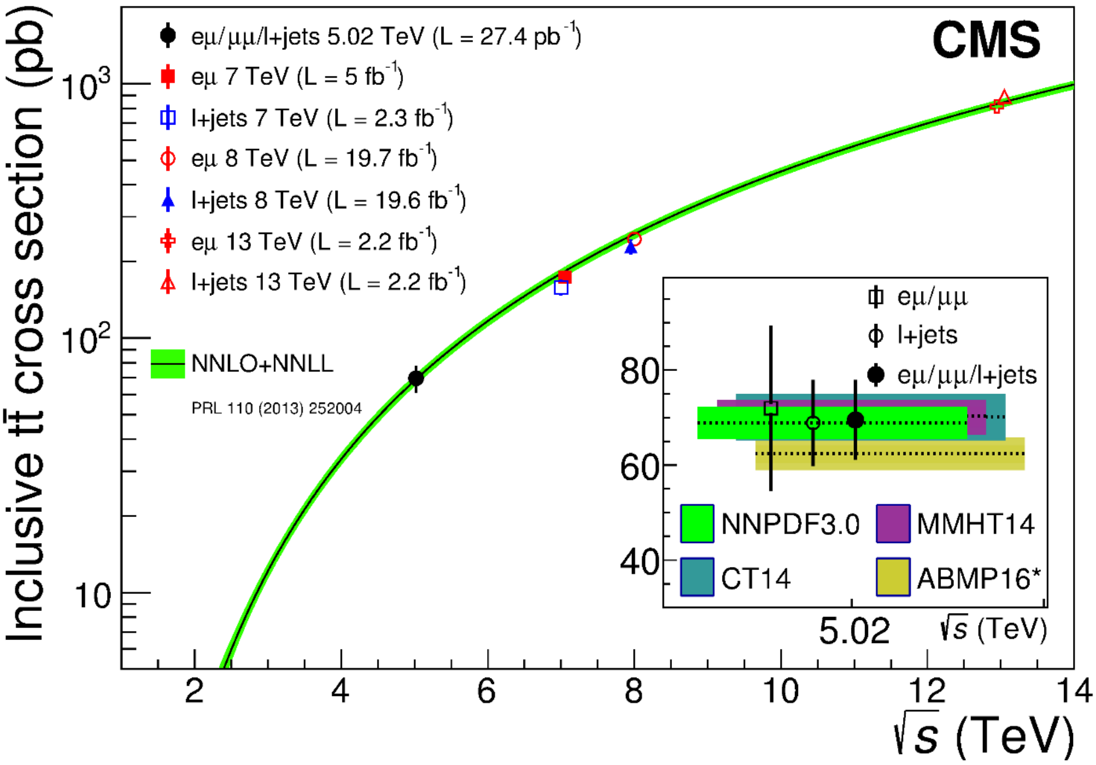

Figure 5. Inclusive $\sigma_{t\bar{t}}$ in pp collisions as a function of the center-of-mass energy; previous CMS measurements at $\sqrt{s} = 7$, 8 [5, 6], and 13 [9, 10] TeV in the separate ℓ+jets and dilepton channels are displayed, along with the combined measurement at 5.02 TeV from this analysis. The NNLO+NNLL theoretical prediction [34] using the NNPDF3.0 [14] PDF set with $\alpha_s(M_Z) = 0.118$ and $m_{top} = 172.5\,\text{GeV}$ is shown in the main plot. In the inset, additional predictions at $\sqrt{s} = 5.02\,\text{TeV}$ using the MMHT14 [54], CT14 [55], and ABMP16 [56] PDF sets, the latter with $\alpha_s(M_Z) = 0.115$ and $m_{top} = 170.4\,\text{GeV}$, are compared, along with the NNPDF3.0 prediction, to the individual and combined results from this analysis. The vertical bars and bands represent the total uncertainties in the data and in the predictions, respectively.

9 QCD analysis

To illustrate the impact of the $\sigma_{t\bar{t}}$ measurements at $\sqrt{s} = 5.02\,\text{TeV}$ on the knowledge of the proton PDFs, the results are used in a QCD analysis at NNLO, together with the combined measurements of neutral- and charged-current cross sections for deep inelastic electron- and positron-proton scattering (DIS) at HERA [57], and the CMS measurement [58] of the muon charge asymmetry in W boson production at $\sqrt{s} = 8\,\text{TeV}$. The latter data set is used in order to improve the constraint on the light-quark distributions.

Version 2.0.0 of xFitter [59, 60], the open-source QCD-analysis framework for PDF determination, is employed, with the partons evolved using the Dokshitzer-Gribov-Lipatov-Altarelli-Parisi equations [61–66] at NNLO, as implemented in the QCDNUM 17-01/13 program [67]. The treatment and the choices for the central values and variations of the c and b quark masses, the strong coupling, and the strange-quark content fraction of the proton follow that of earlier CMS analyses, e.g., ref. [58]. The μ_R, μ_F scales are set to the four-momentum transfer in the case of the DIS data, the W boson mass for the muon charge asymmetry results, and the top quark mass in the case of $\sigma_{\mathrm{t\bar{t}}}$.

The systematic uncertainties in all three measurements of $\sigma_{\mathrm{t\bar{t}}}$ and their correlations are treated the same way as in the combination described in section 8.3. The theoretical predictions for $\sigma_{\mathrm{t\bar{t}}}$ are obtained at NNLO using the HATHOR calculation [68], assuming $m_{\mathrm{top}} = 172.5\,\mathrm{GeV}$. The bin-to-bin correlations of the experimental uncertainties in the muon charge asymmetry and DIS measurements are taken into account. The theoretical predictions for the muon charge asymmetry are obtained as described in ref. [58].

The procedure for the determination of the PDFs follows the approach used in the QCD analysis of ref. [58] and results in a 14-parameter fit. The parametrized PDFs are the gluon distribution, $x\mathrm{g}$, the valence quark distributions, $x\mathrm{u}_v$, $x\mathrm{d}_v$, and the u-type and d-type antiquark distributions, $x\overline{U}$, $x\overline{D}$. The relations $x\overline{U} = x\bar{\mathrm{u}}$ and $x\overline{D} = x\bar{\mathrm{d}} + x\bar{\mathrm{s}}$ are assumed at the initial scale of the QCD evolution $Q_0^2 = 1.9\,\mathrm{GeV}^2$. At this scale, the parametrizations are of the form:

$$x\mathrm{g}(x) = A_{\mathrm{g}} x^{B_{\mathrm{g}}}\,(1-x)^{C_{\mathrm{g}}}\,(1 + D_{\mathrm{g}} x), \tag{9.1}$$

$$x\mathrm{u}_v(x) = A_{\mathrm{u}_v} x^{B_{\mathrm{u}_v}}\,(1-x)^{C_{\mathrm{u}_v}}\,(1 + D_{\mathrm{u}_v} x + E_{\mathrm{u}_v} x^2), \tag{9.2}$$

$$x\mathrm{d}_v(x) = A_{\mathrm{d}_v} x^{B_{\mathrm{d}_v}}\,(1-x)^{C_{\mathrm{d}_v}}, \tag{9.3}$$

$$x\overline{U}(x) = A_{\overline{U}} x^{B_{\overline{U}}}\,(1-x)^{C_{\overline{U}}}\,(1 + E_{\overline{U}} x^2), \tag{9.4}$$

$$x\overline{D}(x) = A_{\overline{D}} x^{B_{\overline{D}}}\,(1-x)^{C_{\overline{D}}}. \tag{9.5}$$

The normalization parameters A_{u_v}, A_{d_v}, and A_{g} are determined by the QCD sum rules, the B parameters are responsible for the small-x behavior of the PDFs, and the C parameters describe the shape of the distribution as $x \to 1$. Additional constraints $B_{\overline{U}} = B_{\overline{D}}$ and $A_{\overline{U}} = A_{\overline{D}}(1 - f_{\mathrm{s}})$ are imposed, with f_{s} being the strangeness fraction, $\bar{\mathrm{s}}/(\bar{\mathrm{d}}+\bar{\mathrm{s}})$, which is set to 0.31 ± 0.08 as in ref. [69], consistent with the value obtained using the CMS measurements of W+c production [70]. Using the measured values for $\sigma_{\mathrm{t\bar{t}}}$ allows the addition of a new free parameter, D_{u_v}, in eq. (9.2), as compared to the analysis in ref. [58].

The predicted and measured cross sections for all the data sets, together with their corresponding uncertainties, are used to build a global χ^2, minimized to determine the PDF parameters [59, 60]. The results of the fit are given in table 5. The quality of the overall fit can be judged based on the global χ^2 divided by the number of degrees of freedom, n_{dof}. For each data set included in the fit, the partial χ^2 divided by the number of the measurements (data points), n_{dp}, is also provided. The correlated part of χ^2, also given in table 5, quantifies the influence of the correlated systematic uncertainties in the fit. The global and partial χ^2 values indicate a general agreement among all the data sets. The somewhat high χ^2/n_{dp} values for the combined DIS data are very similar to those observed in ref. [57], where they are investigated in detail.

The experimental uncertainties in the measurements are propagated to the extracted QCD fit parameters using the MC method [71, 72]. In this method, 400 replicas of pseudo-data are generated, with measured values for $\sigma_{\mathrm{t\bar{t}}}$ allowed to vary within the statistical and systematic uncertainties. For each of them, the PDF fit is performed and the uncertainty

Data sets	Partial χ^2/n_{dp}
HERA neutral current, $\mathrm{e^+p}$, $E_{\mathrm{p}} = 920\,\mathrm{GeV}$	449/377
HERA neutral current, $\mathrm{e^+p}$, $E_{\mathrm{p}} = 820\,\mathrm{GeV}$	71/70
HERA neutral current, $\mathrm{e^+p}$, $E_{\mathrm{p}} = 575\,\mathrm{GeV}$	224/254
HERA neutral current, $\mathrm{e^+p}$, $E_{\mathrm{p}} = 460\,\mathrm{GeV}$	218/204
HERA neutral current, $\mathrm{e^-p}$, $E_{\mathrm{p}} = 920\,\mathrm{GeV}$	218/159
HERA charged current, $\mathrm{e^+p}$, $E_{\mathrm{p}} = 920\,\mathrm{GeV}$	43/39
HERA charged current, $\mathrm{e^-p}$, $E_{\mathrm{p}} = 920\,\mathrm{GeV}$	53/42
CMS $\mathrm{W}^{\pm}$ muon charge asymmetry	2.4/11
CMS $\sigma_{\mathrm{t\bar{t}}}$, $\mathrm{e}^{\pm}\mu^{\mp}$, 5.02 TeV	1.03/1
CMS $\sigma_{\mathrm{t\bar{t}}}$, $\mu^{\pm}\mu^{\mp}$, 5.02 TeV	0.01/1
CMS $\sigma_{\mathrm{t\bar{t}}}$, ℓ+jets, 5.02 TeV	0.70/1
Correlated χ^2	100
Global χ^2/n_{dof}	1387/1145

Table 5. Partial χ^2 per number of data points, n_{dp}, and the global χ^2 per degrees of freedom, n_{dof}, as obtained in the QCD analysis of DIS data, the CMS muon charge asymmetry measurements, and the $\sigma_{\mathrm{t\bar{t}}}$ results at $\sqrt{s} = 5.02\,\mathrm{TeV}$ from this analysis. For the HERA measurements, the energy of the proton beam (E_{p}) is listed for each data set, with the electron/positron energy of 27.5 GeV. The correlated part of the global χ^2 value is also given.

is estimated as the RMS around the central value. In figure 6, the ratio and the relative uncertainties in the gluon distributions, as obtained in the QCD analyses with and without the measured values for $\sigma_{\mathrm{t\bar{t}}}$, are shown. A moderate reduction of the uncertainty in the gluon distribution at $x \gtrsim 0.1$ is observed, once the measured values for $\sigma_{\mathrm{t\bar{t}}}$ are included in the fit. The uncertainties in the valence quark distributions remain unaffected. All changes in the central values of the PDFs are well within the fit uncertainties.

Possible effects from varying the model input parameters and the initial PDF parametrization are investigated in the same way as in the similar analysis of ref. [58]. The two cases when the measured values for $\sigma_{\mathrm{t\bar{t}}}$ are included or excluded from the fit are considered, resulting in the same associated model and parametrization uncertainties.

In conclusion, the $\sigma_{\mathrm{t\bar{t}}}$ measurements at $\sqrt{s} = 5.02\,\mathrm{TeV}$ provide improved uncertainties in the gluon PDF at high x, though the impact is small, owing to the large experimental uncertainties.

10 Summary

The first measurement of the top quark pair ($\mathrm{t\bar{t}}$) production cross section in pp collisions at $\sqrt{s} = 5.02\,\mathrm{TeV}$ is presented for events with one or two leptons and at least two jets, using a data sample collected by the CMS experiment, corresponding to an integrated luminosity of $27.4 \pm 0.6\,\mathrm{pb}^{-1}$. The final measurement is obtained from the combination of the measurements in the individual channels. The result is $\sigma_{\mathrm{t\bar{t}}} = 69.5 \pm 6.1\,(\mathrm{stat}) \pm 5.6\,(\mathrm{syst}) \pm$

JHEP03(2018)115

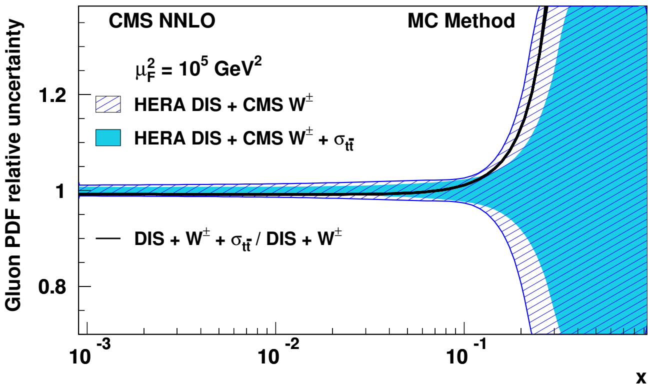

Figure 6. The relative uncertainties in the gluon distribution function of the proton as a function of x at $\mu_F^2 = 10^5\,\mathrm{GeV}^2$ from a QCD analysis using the HERA DIS and CMS muon charge asymmetry measurements (hatched area), and also including the CMS $\sigma_{t\bar{t}}$ results at $\sqrt{s} = 5.02\,\mathrm{TeV}$ (solid area). The relative uncertainties are found after the two gluon distributions have been normalized to unity. The solid line shows the ratio of the gluon distribution function found from the fit with the CMS $\sigma_{t\bar{t}}$ measurements included to that found without.

1.6 (lumi) pb, with a total relative uncertainty of 12%, which is consistent with the standard model prediction. The impact of the measured $t\bar{t}$ cross section in the determination of the parton distribution functions of the proton is studied in a quantum chromodynamics analysis at next-to-next-to-leading order. A moderate decrease of the uncertainty in the gluon distribution is observed at high values of x, the fractional momentum of the proton carried by the gluon.

Acknowledgments

We congratulate our colleagues in the CERN accelerator departments for the excellent performance of the LHC and thank the technical and administrative staffs at CERN and at other CMS institutes for their contributions to the success of the CMS effort. In addition, we gratefully acknowledge the computing centers and personnel of the Worldwide LHC Computing Grid for delivering so effectively the computing infrastructure essential to our analyses. Finally, we acknowledge the enduring support for the construction and operation of the LHC and the CMS detector provided by the following funding agencies: BMWFW and FWF (Austria); FNRS and FWO (Belgium); CNPq, CAPES, FAPERJ, and FAPESP (Brazil); MES (Bulgaria); CERN; CAS, MoST, and NSFC (China); COLCIENCIAS (Colombia); MSES and CSF (Croatia); RPF (Cyprus); SENESCYT (Ecuador); MoER, ERC IUT, and ERDF (Estonia); Academy of Finland, MEC, and HIP (Finland); CEA and CNRS/IN2P3 (France); BMBF, DFG, and HGF (Germany); GSRT (Greece); OTKA and NIH (Hungary); DAE and DST (India); IPM (Iran); SFI (Ireland); INFN (Italy); MSIP and NRF (Republic of Korea); LAS (Lithuania); MOE and UM (Malaysia); BUAP, CINVESTAV, CONACYT, LNS, SEP, and UASLP-FAI (Mexico); MBIE (New Zealand); PAEC (Pakistan); MSHE and NSC (Poland); FCT (Portugal); JINR (Dubna); MON, RosAtom, RAS, RFBR and RAEP (Russia); MESTD (Serbia); SEIDI, CPAN, PCTI and FEDER (Spain); Swiss Funding Agencies (Switzerland); MST (Taipei); ThEPCenter, IPST, STAR, and NSTDA (Thailand); TUBITAK and TAEK (Turkey); NASU and SFFR (Ukraine); STFC (United Kingdom); DOE and NSF (U.S.A.).

Individuals have received support from the Marie-Curie program and the European Research Council and Horizon 2020 Grant, contract No. 675440 (European Union); the Leventis Foundation; the A. P. Sloan Foundation; the Alexander von Humboldt Foundation; the Belgian Federal Science Policy Office; the Fonds pour la Formation à la Recherche dans l'Industrie et dans l'Agriculture (FRIA-Belgium); the Agentschap voor Innovatie door Wetenschap en Technologie (IWT-Belgium); the Ministry of Education, Youth and Sports (MEYS) of the Czech Republic; the Council of Science and Industrial Research, India; the HOMING PLUS program of the Foundation for Polish Science, cofinanced from European Union, Regional Development Fund, the Mobility Plus program of the Ministry of Science and Higher Education, the National Science Center (Poland), contracts Harmonia 2014/14/M/ST2/00428, Opus 2014/13/B/ST2/02543, 2014/15/B/ST2/03998, and 2015/19/B/ST2/02861, Sonata-bis 2012/07/E/ST2/01406; the National Priorities Research Program by Qatar National Research Fund; the Programa Severo Ochoa del Principado de Asturias; the Thalis and Aristeia programs cofinanced by EU-ESF and the Greek NSRF; the Rachadapisek Sompot Fund for Postdoctoral Fellowship, Chulalongkorn University and the Chulalongkorn Academic into Its 2nd Century Project Advancement Project (Thailand); the Welch Foundation, contract C-1845; and the Weston Havens Foundation (U.S.A.).

Open Access. This article is distributed under the terms of the Creative Commons Attribution License (CC-BY 4.0), which permits any use, distribution and reproduction in any medium, provided the original author(s) and source are credited.

References

[1] CMS collaboration, *Determination of the top-quark pole mass and strong coupling constant from the $t\bar{t}$ production cross section in pp collisions at $\sqrt{s} = 7$ TeV*, *Phys. Lett.* **B 728** (2014) 496 [*Erratum ibid.* **B 738** (2014) 526] [`arXiv:1307.1907`] [INSPIRE].

[2] CMS collaboration, *Measurement of double-differential cross sections for top quark pair production in pp collisions at $\sqrt{s} = 8$ TeV and impact on parton distribution functions*, *Eur. Phys. J.* **C 77** (2017) 459 [`arXiv:1703.01630`] [INSPIRE].

[3] ATLAS collaboration, *Measurement of the top quark pair production cross-section with ATLAS in the single lepton channel*, *Phys. Lett.* **B 711** (2012) 244 [`arXiv:1201.1889`] [INSPIRE].

[4] ATLAS collaboration, *Measurement of the $t\bar{t}$ production cross-section using $e\mu$ events with b-tagged jets in pp collisions at $\sqrt{s} = 7$ and 8 TeV with the ATLAS detector*, *Eur. Phys. J.* **C 74** (2014) 3109 [`arXiv:1406.5375`] [INSPIRE].

[5] CMS collaboration, *Measurement of the $t\bar{t}$ production cross section in the e-μ channel in proton-proton collisions at $\sqrt{s} = 7$ and 8 TeV*, *JHEP* **08** (2016) 029 [`arXiv:1603.02303`] [INSPIRE].

[6] CMS collaboration, *Measurements of the $t\bar{t}$ production cross section in lepton+jets final states in pp collisions at 8 TeV and ratio of 8 to 7 TeV cross sections*, *Eur. Phys. J.* **C 77** (2017) 15 [`arXiv:1602.09024`] [INSPIRE].

[7] ATLAS collaboration, *Measurement of the $t\bar{t}$ production cross-section using $e\mu$ events with b-tagged jets in pp collisions at $\sqrt{s} = 13$ TeV with the ATLAS detector*, *Phys. Lett.* **B 761** (2016) 136 [*Erratum ibid.* **B 772** (2017) 879] [`arXiv:1606.02699`] [INSPIRE].

[8] CMS collaboration, *Measurement of the top quark pair production cross section in proton-proton collisions at $\sqrt{s} = 13$ TeV*, *Phys. Rev. Lett.* **116** (2016) 052002 [`arXiv:1510.05302`] [INSPIRE].

[9] CMS collaboration, *Measurement of the $t\bar{t}$ production cross section using events in the $e\mu$ final state in pp collisions at $\sqrt{s} = 13$ TeV*, *Eur. Phys. J.* **C 77** (2017) 172 [`arXiv:1611.04040`] [INSPIRE].

[10] CMS collaboration, *Measurement of the $t\bar{t}$ production cross section using events with one lepton and at least one jet in pp collisions at $\sqrt{s} = 13$ TeV*, *JHEP* **09** (2017) 051 [`arXiv:1701.06228`] [INSPIRE].

[11] S. Frixione, P. Nason and C. Oleari, *Matching NLO QCD computations with Parton Shower simulations: the POWHEG method*, *JHEP* **11** (2007) 070 [`arXiv:0709.2092`] [INSPIRE].

[12] S. Alioli, P. Nason, C. Oleari and E. Re, *A general framework for implementing NLO calculations in shower Monte Carlo programs: the POWHEG BOX*, *JHEP* **06** (2010) 043 [`arXiv:1002.2581`] [INSPIRE].

[13] S. Frixione, P. Nason and G. Ridolfi, *A positive-weight next-to-leading-order Monte Carlo for heavy flavour hadroproduction*, *JHEP* **09** (2007) 126 [`arXiv:0707.3088`] [INSPIRE].

[14] NNPDF collaboration, R.D. Ball et al., *Parton distributions for the LHC Run II*, *JHEP* **04** (2015) 040 [`arXiv:1410.8849`] [INSPIRE].

[15] D. d'Enterria, K. Krajczár and H. Paukkunen, *Top-quark production in proton–nucleus and nucleus–nucleus collisions at LHC energies and beyond*, *Phys. Lett.* **B 746** (2015) 64 [`arXiv:1501.05879`] [INSPIRE].

[16] CMS collaboration, *Projections for heavy ions with HL-LHC*, CMS-PAS-FTR-13-025 (2013).

[17] CMS collaboration, *Observation of top quark production in proton-nucleus collisions*, *Phys. Rev. Lett.* **119** (2017) 242001 [`arXiv:1709.07411`] [INSPIRE].

[18] CMS collaboration, *The CMS trigger system*, 2017 *JINST* **12** P01020 [`arXiv:1609.02366`] [INSPIRE].

[19] CMS collaboration, *The CMS experiment at the CERN LHC*, 2008 *JINST* **3** S08004 [INSPIRE].

[20] CMS Collaboration, *CMS luminosity calibration for the pp reference run at $\sqrt{s} = 5.02$ TeV*, CMS-PAS-LUM-16-001 (2016).

[21] T. Sjöstrand, S. Mrenna and P.Z. Skands, *PYTHIA 6.4 physics and manual*, *JHEP* **05** (2006) 026 [`hep-ph/0603175`] [INSPIRE].

[22] T. Sjöstrand et al., *An introduction to PYTHIA 8.2*, *Comput. Phys. Commun.* **191** (2015) 159 [`arXiv:1410.3012`] [INSPIRE].

[23] CMS collaboration, *Event generator tunes obtained from underlying event and multiparton scattering measurements*, *Eur. Phys. J.* **C 76** (2016) 155 [`arXiv:1512.00815`] [INSPIRE].

[24] P. Skands, S. Carrazza and J. Rojo, *Tuning PYTHIA 8.1: the Monash 2013 Tune*, *Eur. Phys. J.* **C 74** (2014) 3024 [`arXiv:1404.5630`] [INSPIRE].

[25] J. Alwall et al., *The automated computation of tree-level and next-to-leading order differential cross sections and their matching to parton shower simulations*, *JHEP* **07** (2014) 079 [`arXiv:1405.0301`] [INSPIRE].

[26] R. Frederix and S. Frixione, *Merging meets matching in MC@NLO*, *JHEP* **12** (2012) 061 [`arXiv:1209.6215`] [INSPIRE].

[27] K. Melnikov and F. Petriello, *Electroweak gauge boson production at hadron colliders through* $O(\alpha_s^2)$, *Phys. Rev.* **D 74** (2006) 114017 [`hep-ph/0609070`] [INSPIRE].

[28] S. Alioli, P. Nason, C. Oleari and E. Re, *NLO single-top production matched with shower in POWHEG: s- and t-channel contributions*, *JHEP* **09** (2009) 111 [*Erratum ibid.* **02** (2010) 011] [`arXiv:0907.4076`] [INSPIRE].

[29] E. Re, *Single-top Wt-channel production matched with parton showers using the POWHEG method*, *Eur. Phys. J.* **C 71** (2011) 1547 [`arXiv:1009.2450`] [INSPIRE].

[30] N. Kidonakis, *Top quark production*, in the proceedings of the *Helmholtz International Summer School on Physics of Heavy Quarks and Hadrons (HQ 2013)*, July 15–28, Dubna, Russia (2013), `arXiv:1311.0283` [INSPIRE].

[31] J.M. Campbell and R.K. Ellis, *MCFM for the Tevatron and the LHC*, *Nucl. Phys. Proc. Suppl.* **205-206** (2010) 10 [`arXiv:1007.3492`] [INSPIRE].

[32] GEANT4 collaboration, S. Agostinelli et al., *GEANT4 – a simulation toolkit*, *Nucl. Instrum. Meth.* **A 506** (2003) 250 [INSPIRE].

[33] M. Czakon and A. Mitov, TOP++*: a program for the calculation of the top-pair cross-section at hadron colliders*, *Comput. Phys. Commun.* **185** (2014) 2930 [`arXiv:1112.5675`] [INSPIRE].

[34] M. Czakon, P. Fiedler and A. Mitov, *Total top-quark pair-production cross section at hadron colliders through* $O(\alpha_s^4)$, *Phys. Rev. Lett.* **110** (2013) 252004 [`arXiv:1303.6254`] [INSPIRE].

[35] E. Todesco and J. Wenninger, *Large hadron collider momentum calibration and accuracy*, *Phys. Rev. Accel. Beams* **20** (2017) 081003 [INSPIRE].

[36] CMS collaboration, *Particle-flow reconstruction and global event description with the CMS detector*, 2017 *JINST* **12** P10003 [`arXiv:1706.04965`] [INSPIRE].

[37] CMS collaboration, *Performance of electron reconstruction and selection with the CMS detector in proton-proton collisions at* $\sqrt{s} = 8$ *TeV*, 2015 *JINST* **10** P06005 [`arXiv:1502.02701`] [INSPIRE].

[38] CMS collaboration, *Performance of CMS muon reconstruction in pp collision events at* $\sqrt{s} = 7$ *TeV*, 2012 *JINST* **7** P10002 [`arXiv:1206.4071`] [INSPIRE].

[39] CMS collaboration, *The performance of the CMS muon detector in proton-proton collisions at* $\sqrt{s} = 7$ *TeV at the LHC*, 2013 *JINST* **8** P11002 [`arXiv:1306.6905`] [INSPIRE].

[40] CMS collaboration, *Performance of missing energy reconstruction in 13 TeV pp collision data using the CMS detector*, CMS-PAS-JME-16-004 (2016).

[41] M. Cacciari, G.P. Salam and G. Soyez, *The anti-*k_t *jet clustering algorithm*, *JHEP* **04** (2008) 063 [`arXiv:0802.1189`] [INSPIRE].

[42] M. Cacciari, G.P. Salam and G. Soyez, *FastJet user manual*, *Eur. Phys. J.* **C 72** (2012) 1896 [`arXiv:1111.6097`] [INSPIRE].

[43] M. Cacciari and G.P. Salam, *Pileup subtraction using jet areas*, *Phys. Lett.* **B 659** (2008) 119 [arXiv:0707.1378] [INSPIRE].

[44] CMS collaboration, *Measurements of inclusive W and Z cross sections in pp collisions at $\sqrt{s} = 7$ TeV*, *JHEP* **01** (2011) 080 [arXiv:1012.2466] [INSPIRE].

[45] CMS collaboration, *Determination of jet energy calibration and transverse momentum resolution in CMS*, 2011 *JINST* **6** P11002 [arXiv:1107.4277] [INSPIRE].

[46] CMS collaboration, *Identification of heavy-flavour jets with the CMS detector in pp collisions at* 13 *TeV*, submitted to *JINST* (2017), arXiv:1712.07158 [INSPIRE].

[47] CMS collaboration, *First measurement of the cross section for top-quark pair production in proton-proton collisions at $\sqrt{s} = 7$ TeV*, *Phys. Lett.* **B 695** (2011) 424 [arXiv:1010.5994] [INSPIRE].

[48] CMS collaboration, *Jet energy scale and resolution in the CMS experiment in pp collisions at* 8 *TeV*, 2017 *JINST* **12** P02014 [arXiv:1607.03663] [INSPIRE].

[49] M. Bahr et al., *HERWIG++ physics and manual*, *Eur. Phys. J.* **C 58** (2008) 639 [arXiv:0803.0883] [INSPIRE].

[50] G. Cowan, K. Cranmer, E. Gross and O. Vitells, *Asymptotic formulae for likelihood-based tests of new physics*, *Eur. Phys. J.* **C 71** (2011) 1554 [*Erratum ibid.* **C 73** (2013) 2501] [arXiv:1007.1727] [INSPIRE].

[51] L. Lyons, D. Gibaut and P. Clifford, *How to combine correlated estimates of a single physical quantity*, *Nucl. Instrum. Meth.* **A 270** (1988) 110 [INSPIRE].

[52] A. Valassi and R. Chierici, *Information and treatment of unknown correlations in the combination of measurements using the BLUE method*, *Eur. Phys. J.* **C 74** (2014) 2717 [arXiv:1307.4003] [INSPIRE].

[53] L. Lista, *The bias of the unbiased estimator: a study of the iterative application of the BLUE method*, *Nucl. Instrum. Meth.* **A 764** (2014) 82 [*Erratum ibid.* **A 773** (2015) 87] [arXiv:1405.3425] [INSPIRE].

[54] L.A. Harland-Lang, A.D. Martin, P. Motylinski and R.S. Thorne, *Parton distributions in the LHC era: MMHT 2014 PDFs*, *Eur. Phys. J.* **C 75** (2015) 204 [arXiv:1412.3989] [INSPIRE].

[55] S. Dulat et al., *New parton distribution functions from a global analysis of quantum chromodynamics*, *Phys. Rev.* **D 93** (2016) 033006 [arXiv:1506.07443] [INSPIRE].

[56] S. Alekhin, J. Blümlein, S. Moch and R. Placakyte, *Parton distribution functions, α_s and heavy-quark masses for LHC Run II*, *Phys. Rev.* **D 96** (2017) 014011 [arXiv:1701.05838] [INSPIRE].

[57] ZEUS, H1 collaboration, H. Abramowicz et al., *Combination of measurements of inclusive deep inelastic $e^{\pm}p$ scattering cross sections and QCD analysis of HERA data*, *Eur. Phys. J.* **C 75** (2015) 580 [arXiv:1506.06042] [INSPIRE].

[58] CMS collaboration, *Measurement of the differential cross section and charge asymmetry for inclusive $pp \to W^{\pm} + X$ production at $\sqrt{s} = 8$ TeV*, *Eur. Phys. J.* **C 76** (2016) 469 [arXiv:1603.01803] [INSPIRE].

[59] S. Alekhin et al., *HERAFitter*, *Eur. Phys. J.* **C 75** (2015) 304 [arXiv:1410.4412] [INSPIRE].

[60] xFitter collaboration, http://www.xfitter.org.

[61] V.N. Gribov and L.N. Lipatov, *Deep inelastic ep scattering in perturbation theory*, *Sov. J. Nucl. Phys.* **15** (1972) 438 [INSPIRE].

[62] G. Altarelli and G. Parisi, *Asymptotic freedom in parton language*, *Nucl. Phys.* **B 126** (1977) 298 [INSPIRE].

[63] G. Curci, W. Furmanski and R. Petronzio, *Evolution of parton densities beyond leading order: the nonsinglet case*, *Nucl. Phys.* **B 175** (1980) 27 [INSPIRE].

[64] W. Furmanski and R. Petronzio, *Singlet parton densities beyond leading order*, *Phys. Lett.* **97B** (1980) 437 [INSPIRE].

[65] S. Moch, J.A.M. Vermaseren and A. Vogt, *The three loop splitting functions in QCD: the nonsinglet case*, *Nucl. Phys.* **B 688** (2004) 101 [`hep-ph/0403192`] [INSPIRE].

[66] A. Vogt, S. Moch and J.A.M. Vermaseren, *The three-loop splitting functions in QCD: the singlet case*, *Nucl. Phys.* **B 691** (2004) 129 [`hep-ph/0404111`] [INSPIRE].

[67] M. Botje, *QCDNUM: fast QCD evolution and convolution*, *Comput. Phys. Commun.* **182** (2011) 490 [`arXiv:1005.1481`] [INSPIRE].

[68] M. Aliev et al., *HATHOR: HAdronic Top and Heavy quarks crOss section calculatoR*, *Comput. Phys. Commun.* **182** (2011) 1034 [`arXiv:1007.1327`] [INSPIRE].

[69] A.D. Martin, W.J. Stirling, R.S. Thorne and G. Watt, *Parton distributions for the LHC*, *Eur. Phys. J.* **C 63** (2009) 189 [`arXiv:0901.0002`] [INSPIRE].

[70] CMS collaboration, *Measurement of the muon charge asymmetry in inclusive $pp \to W + X$ production at $\sqrt{s} = 7$ TeV and an improved determination of light parton distribution functions*, *Phys. Rev.* **D 90** (2014) 032004 [`arXiv:1312.6283`] [INSPIRE].

[71] W.T. Giele and S. Keller, *Implications of hadron collider observables on parton distribution function uncertainties*, *Phys. Rev.* **D 58** (1998) 094023 [`hep-ph/9803393`] [INSPIRE].

[72] W.T. Giele, S.A. Keller and D.A. Kosower, *Parton distribution function uncertainties*, `hep-ph/0104052` [INSPIRE].

The CMS collaboration

Yerevan Physics Institute, Yerevan, Armenia

A.M. Sirunyan, A. Tumasyan

Institut für Hochenergiephysik, Wien, Austria

W. Adam, F. Ambrogi, E. Asilar, T. Bergauer, J. Brandstetter, E. Brondolin, M. Dragicevic, J. Erö, M. Flechl, M. Friedl, R. Frühwirth[1], V.M. Ghete, J. Grossmann, J. Hrubec, M. Jeitler[1], A. König, N. Krammer, I. Krätschmer, D. Liko, T. Madlener, I. Mikulec, E. Pree, D. Rabady, N. Rad, H. Rohringer, J. Schieck[1], R. Schöfbeck, M. Spanring, D. Spitzbart, W. Waltenberger, J. Wittmann, C.-E. Wulz[1], M. Zarucki

Institute for Nuclear Problems, Minsk, Belarus

V. Chekhovsky, V. Mossolov, J. Suarez Gonzalez

Universiteit Antwerpen, Antwerpen, Belgium

E.A. De Wolf, D. Di Croce, X. Janssen, J. Lauwers, M. Van De Klundert, H. Van Haevermaet, P. Van Mechelen, N. Van Remortel

Vrije Universiteit Brussel, Brussel, Belgium

S. Abu Zeid, F. Blekman, J. D'Hondt, I. De Bruyn, J. De Clercq, K. Deroover, G. Flouris, D. Lontkovskyi, S. Lowette, S. Moortgat, L. Moreels, Q. Python, K. Skovpen, S. Tavernier, W. Van Doninck, P. Van Mulders, I. Van Parijs

Université Libre de Bruxelles, Bruxelles, Belgium

H. Brun, B. Clerbaux, G. De Lentdecker, H. Delannoy, G. Fasanella, L. Favart, R. Goldouzian, A. Grebenyuk, G. Karapostoli, T. Lenzi, J. Luetic, T. Maerschalk, A. Marinov, A. Randle-conde, T. Seva, C. Vander Velde, P. Vanlaer, D. Vannerom, R. Yonamine, F. Zenoni, F. Zhang[2]

Ghent University, Ghent, Belgium

A. Cimmino, T. Cornelis, D. Dobur, A. Fagot, M. Gul, I. Khvastunov, D. Poyraz, C. Roskas, S. Salva, M. Tytgat, W. Verbeke, N. Zaganidis

Université Catholique de Louvain, Louvain-la-Neuve, Belgium

H. Bakhshiansohi, O. Bondu, S. Brochet, G. Bruno, C. Caputo, A. Caudron, S. De Visscher, C. Delaere, M. Delcourt, B. Francois, A. Giammanco, A. Jafari, M. Komm, G. Krintiras, V. Lemaitre, A. Magitteri, A. Mertens, M. Musich, K. Piotrzkowski, L. Quertenmont, M. Vidal Marono, S. Wertz

Université de Mons, Mons, Belgium

N. Beliy

Centro Brasileiro de Pesquisas Fisicas, Rio de Janeiro, Brazil

W.L. Aldá Júnior, F.L. Alves, G.A. Alves, L. Brito, M. Correa Martins Junior, C. Hensel, A. Moraes, M.E. Pol, P. Rebello Teles

JHEP03(2018)115

Universidade do Estado do Rio de Janeiro, Rio de Janeiro, Brazil
E. Belchior Batista Das Chagas, W. Carvalho, J. Chinellato[3], A. Custódio, E.M. Da Costa, G.G. Da Silveira[4], D. De Jesus Damiao, S. Fonseca De Souza, L.M. Huertas Guativa, H. Malbouisson, M. Melo De Almeida, C. Mora Herrera, L. Mundim, H. Nogima, A. Santoro, A. Sznajder, E.J. Tonelli Manganote[3], F. Torres Da Silva De Araujo, A. Vilela Pereira

Universidade Estadual Paulista [a], Universidade Federal do ABC [b], São Paulo, Brazil
S. Ahuja[a], C.A. Bernardes[a], T.R. Fernandez Perez Tomei[a], E.M. Gregores[b], P.G. Mercadante[b], S.F. Novaes[a], Sandra S. Padula[a], D. Romero Abad[b], J.C. Ruiz Vargas[a]

Institute for Nuclear Research and Nuclear Energy, Bulgarian Academy of Sciences, Sofia, Bulgaria
A. Aleksandrov, R. Hadjiiska, P. Iaydjiev, M. Misheva, M. Rodozov, M. Shopova, S. Stoykova, G. Sultanov

University of Sofia, Sofia, Bulgaria
A. Dimitrov, I. Glushkov, L. Litov, B. Pavlov, P. Petkov

Beihang University, Beijing, China
W. Fang[5], X. Gao[5]

Institute of High Energy Physics, Beijing, China
M. Ahmad, J.G. Bian, G.M. Chen, H.S. Chen, M. Chen, Y. Chen, C.H. Jiang, D. Leggat, H. Liao, Z. Liu, F. Romeo, S.M. Shaheen, A. Spiezia, J. Tao, C. Wang, Z. Wang, E. Yazgan, H. Zhang, S. Zhang, J. Zhao

State Key Laboratory of Nuclear Physics and Technology, Peking University, Beijing, China
Y. Ban, G. Chen, Q. Li, S. Liu, Y. Mao, S.J. Qian, D. Wang, Z. Xu

Universidad de Los Andes, Bogota, Colombia
C. Avila, A. Cabrera, L.F. Chaparro Sierra, C. Florez, C.F. González Hernández, J.D. Ruiz Alvarez

University of Split, Faculty of Electrical Engineering, Mechanical Engineering and Naval Architecture, Split, Croatia
B. Courbon, N. Godinovic, D. Lelas, I. Puljak, P.M. Ribeiro Cipriano, T. Sculac

University of Split, Faculty of Science, Split, Croatia
Z. Antunovic, M. Kovac

Institute Rudjer Boskovic, Zagreb, Croatia
V. Brigljevic, D. Ferencek, K. Kadija, B. Mesic, A. Starodumov[6], T. Susa

University of Cyprus, Nicosia, Cyprus
M.W. Ather, A. Attikis, G. Mavromanolakis, J. Mousa, C. Nicolaou, F. Ptochos, P.A. Razis, H. Rykaczewski

Charles University, Prague, Czech Republic
M. Finger[7], M. Finger Jr.[7]

Universidad San Francisco de Quito, Quito, Ecuador
E. Carrera Jarrin

Academy of Scientific Research and Technology of the Arab Republic of Egypt, Egyptian Network of High Energy Physics, Cairo, Egypt
Y. Assran[8,9], M.A. Mahmoud[10,9], A. Mahrous[11]

National Institute of Chemical Physics and Biophysics, Tallinn, Estonia
R.K. Dewanjee, M. Kadastik, L. Perrini, M. Raidal, A. Tiko, C. Veelken

Department of Physics, University of Helsinki, Helsinki, Finland
P. Eerola, J. Pekkanen, M. Voutilainen

Helsinki Institute of Physics, Helsinki, Finland
J. Härkönen, T. Järvinen, V. Karimäki, R. Kinnunen, T. Lampén, K. Lassila-Perini, S. Lehti, T. Lindén, P. Luukka, E. Tuominen, J. Tuominiemi, E. Tuovinen

Lappeenranta University of Technology, Lappeenranta, Finland
J. Talvitie, T. Tuuva

IRFU, CEA, Université Paris-Saclay, Gif-sur-Yvette, France
M. Besancon, F. Couderc, M. Dejardin, D. Denegri, J.L. Faure, F. Ferri, S. Ganjour, S. Ghosh, A. Givernaud, P. Gras, G. Hamel de Monchenault, P. Jarry, I. Kucher, E. Locci, M. Machet, J. Malcles, G. Negro, J. Rander, A. Rosowsky, M.Ö. Sahin, M. Titov

Laboratoire Leprince-Ringuet, Ecole polytechnique, CNRS/IN2P3, Université Paris-Saclay, Palaiseau, France
A. Abdulsalam, I. Antropov, S. Baffioni, F. Beaudette, P. Busson, L. Cadamuro, C. Charlot, R. Granier de Cassagnac, M. Jo, S. Lisniak, A. Lobanov, J. Martin Blanco, M. Nguyen, C. Ochando, G. Ortona, P. Paganini, P. Pigard, S. Regnard, R. Salerno, J.B. Sauvan, Y. Sirois, A.G. Stahl Leiton, T. Strebler, Y. Yilmaz, A. Zabi, A. Zghiche

Université de Strasbourg, CNRS, IPHC UMR 7178, F-67000 Strasbourg, France
J.-L. Agram[12], J. Andrea, D. Bloch, J.-M. Brom, M. Buttignol, E.C. Chabert, N. Chanon, C. Collard, E. Conte[12], X. Coubez, J.-C. Fontaine[12], D. Gelé, U. Goerlach, M. Jansová, A.-C. Le Bihan, N. Tonon, P. Van Hove

Centre de Calcul de l'Institut National de Physique Nucleaire et de Physique des Particules, CNRS/IN2P3, Villeurbanne, France
S. Gadrat

Université de Lyon, Université Claude Bernard Lyon 1, CNRS-IN2P3, Institut de Physique Nucléaire de Lyon, Villeurbanne, France
S. Beauceron, C. Bernet, G. Boudoul, R. Chierici, D. Contardo, P. Depasse, H. El Mamouni, J. Fay, L. Finco, S. Gascon, M. Gouzevitch, G. Grenier, B. Ille, F. Lagarde, I.B. Laktineh,

M. Lethuillier, L. Mirabito, A.L. Pequegnot, S. Perries, A. Popov[13], V. Sordini, M. Vander Donckt, S. Viret

Georgian Technical University, Tbilisi, Georgia
A. Khvedelidze[7]

Tbilisi State University, Tbilisi, Georgia
D. Lomidze

RWTH Aachen University, I. Physikalisches Institut, Aachen, Germany
C. Autermann, S. Beranek, L. Feld, M.K. Kiesel, K. Klein, M. Lipinski, M. Preuten, C. Schomakers, J. Schulz, T. Verlage, V. Zhukov[13]

RWTH Aachen University, III. Physikalisches Institut A, Aachen, Germany
A. Albert, E. Dietz-Laursonn, D. Duchardt, M. Endres, M. Erdmann, S. Erdweg, T. Esch, R. Fischer, A. Güth, M. Hamer, T. Hebbeker, C. Heidemann, K. Hoepfner, S. Knutzen, M. Merschmeyer, A. Meyer, P. Millet, S. Mukherjee, M. Olschewski, K. Padeken, T. Pook, M. Radziej, H. Reithler, M. Rieger, F. Scheuch, D. Teyssier, S. Thüer

RWTH Aachen University, III. Physikalisches Institut B, Aachen, Germany
G. Flügge, B. Kargoll, T. Kress, A. Künsken, J. Lingemann, T. Müller, A. Nehrkorn, A. Nowack, C. Pistone, O. Pooth, A. Stahl[14]

Deutsches Elektronen-Synchrotron, Hamburg, Germany
M. Aldaya Martin, T. Arndt, C. Asawatangtrakuldee, K. Beernaert, O. Behnke, U. Behrens, A. Bermúdez Martínez, A.A. Bin Anuar, K. Borras[15], V. Botta, A. Campbell, P. Connor, C. Contreras-Campana, F. Costanza, C. Diez Pardos, G. Eckerlin, D. Eckstein, T. Eichhorn, E. Eren, E. Gallo[16], J. Garay Garcia, A. Geiser, A. Gizhko, J.M. Grados Luyando, A. Grohsjean, P. Gunnellini, M. Guthoff, A. Harb, J. Hauk, M. Hempel[17], H. Jung, A. Kalogeropoulos, M. Kasemann, J. Keaveney, C. Kleinwort, I. Korol, D. Krücker, W. Lange, A. Lelek, T. Lenz, J. Leonard, K. Lipka, W. Lohmann[17], R. Mankel, I.-A. Melzer-Pellmann, A.B. Meyer, G. Mittag, J. Mnich, A. Mussgiller, E. Ntomari, D. Pitzl, A. Raspereza, B. Roland, M. Savitskyi, P. Saxena, R. Shevchenko, S. Spannagel, N. Stefaniuk, G.P. Van Onsem, R. Walsh, Y. Wen, K. Wichmann, C. Wissing, O. Zenaiev

University of Hamburg, Hamburg, Germany
S. Bein, V. Blobel, M. Centis Vignali, T. Dreyer, E. Garutti, D. Gonzalez, J. Haller, A. Hinzmann, M. Hoffmann, A. Karavdina, R. Klanner, R. Kogler, N. Kovalchuk, S. Kurz, T. Lapsien, I. Marchesini, D. Marconi, M. Meyer, M. Niedziela, D. Nowatschin, F. Pantaleo[14], T. Peiffer, A. Perieanu, C. Scharf, P. Schleper, A. Schmidt, S. Schumann, J. Schwandt, J. Sonneveld, H. Stadie, G. Steinbrück, F.M. Stober, M. Stöver, H. Tholen, D. Troendle, E. Usai, L. Vanelderen, A. Vanhoefer, B. Vormwald

Institut für Experimentelle Kernphysik, Karlsruhe, Germany
M. Akbiyik, C. Barth, S. Baur, E. Butz, R. Caspart, T. Chwalek, F. Colombo, W. De Boer, A. Dierlamm, B. Freund, R. Friese, M. Giffels, A. Gilbert, D. Haitz, F. Hartmann[14],

S.M. Heindl, U. Husemann, F. Kassel[14], S. Kudella, H. Mildner, M.U. Mozer, Th. Müller, M. Plagge, G. Quast, K. Rabbertz, M. Schröder, I. Shvetsov, G. Sieber, H.J. Simonis, R. Ulrich, S. Wayand, M. Weber, T. Weiler, S. Williamson, C. Wöhrmann, R. Wolf

Institute of Nuclear and Particle Physics (INPP), NCSR Demokritos, Aghia Paraskevi, Greece

G. Anagnostou, G. Daskalakis, T. Geralis, V.A. Giakoumopoulou, A. Kyriakis, D. Loukas, I. Topsis-Giotis

National and Kapodistrian University of Athens, Athens, Greece

G. Karathanasis, S. Kesisoglou, A. Panagiotou, N. Saoulidou

National Technical University of Athens, Athens, Greece

K. Kousouris

University of Ioánnina, Ioánnina, Greece

I. Evangelou, C. Foudas, P. Kokkas, S. Mallios, N. Manthos, I. Papadopoulos, E. Paradas, J. Strologas, F.A. Triantis

MTA-ELTE Lendület CMS Particle and Nuclear Physics Group, Eötvös Loránd University, Budapest, Hungary

M. Csanad, N. Filipovic, G. Pasztor, G.I. Veres[18]

Wigner Research Centre for Physics, Budapest, Hungary

G. Bencze, C. Hajdu, D. Horvath[19], Á. Hunyadi, F. Sikler, V. Veszpremi, A.J. Zsigmond

Institute of Nuclear Research ATOMKI, Debrecen, Hungary

N. Beni, S. Czellar, J. Karancsi[20], A. Makovec, J. Molnar, Z. Szillasi

Institute of Physics, University of Debrecen, Debrecen, Hungary

M. Bartók[18], P. Raics, Z.L. Trocsanyi, B. Ujvari

Indian Institute of Science (IISc), Bangalore, India

S. Choudhury, J.R. Komaragiri

National Institute of Science Education and Research, Bhubaneswar, India

S. Bahinipati[21], S. Bhowmik, P. Mal, K. Mandal, A. Nayak[22], D.K. Sahoo[21], N. Sahoo, S.K. Swain

Panjab University, Chandigarh, India

S. Bansal, S.B. Beri, V. Bhatnagar, R. Chawla, N. Dhingra, A.K. Kalsi, A. Kaur, M. Kaur, R. Kumar, P. Kumari, A. Mehta, J.B. Singh, G. Walia

University of Delhi, Delhi, India

Ashok Kumar, Aashaq Shah, A. Bhardwaj, S. Chauhan, B.C. Choudhary, R.B. Garg, S. Keshri, A. Kumar, S. Malhotra, M. Naimuddin, K. Ranjan, R. Sharma

Saha Institute of Nuclear Physics, HBNI, Kolkata, India

R. Bhardwaj, R. Bhattacharya, S. Bhattacharya, U. Bhawandeep, S. Dey, S. Dutt, S. Dutta, S. Ghosh, N. Majumdar, A. Modak, K. Mondal, S. Mukhopadhyay, S. Nandan, A. Purohit, A. Roy, D. Roy, S. Roy Chowdhury, S. Sarkar, M. Sharan, S. Thakur

JHEP03(2018)115

Indian Institute of Technology Madras, Madras, India

P.K. Behera

Bhabha Atomic Research Centre, Mumbai, India

R. Chudasama, D. Dutta, V. Jha, V. Kumar, A.K. Mohanty[14], P.K. Netrakanti, L.M. Pant, P. Shukla, A. Topkar

Tata Institute of Fundamental Research-A, Mumbai, India

T. Aziz, S. Dugad, B. Mahakud, S. Mitra, G.B. Mohanty, N. Sur, B. Sutar

Tata Institute of Fundamental Research-B, Mumbai, India

S. Banerjee, S. Bhattacharya, S. Chatterjee, P. Das, M. Guchait, Sa. Jain, S. Kumar, M. Maity[23], G. Majumder, K. Mazumdar, T. Sarkar[23], N. Wickramage[24]

Indian Institute of Science Education and Research (IISER), Pune, India

S. Chauhan, S. Dube, V. Hegde, A. Kapoor, K. Kothekar, S. Pandey, A. Rane, S. Sharma

Institute for Research in Fundamental Sciences (IPM), Tehran, Iran

S. Chenarani[25], E. Eskandari Tadavani, S.M. Etesami[25], M. Khakzad, M. Mohammadi Najafabadi, M. Naseri, S. Paktinat Mehdiabadi[26], F. Rezaei Hosseinabadi, B. Safarzadeh[27], M. Zeinali

University College Dublin, Dublin, Ireland

M. Felcini, M. Grunewald

INFN Sezione di Bari [a], Università di Bari [b], Politecnico di Bari [c], Bari, Italy

M. Abbrescia[a,b], C. Calabria[a,b], A. Colaleo[a], D. Creanza[a,c], L. Cristella[a,b], N. De Filippis[a,c], M. De Palma[a,b], F. Errico[a,b], L. Fiore[a], G. Iaselli[a,c], S. Lezki[a,b], G. Maggi[a,c], M. Maggi[a], G. Miniello[a,b], S. My[a,b], S. Nuzzo[a,b], A. Pompili[a,b], G. Pugliese[a,c], R. Radogna[a], A. Ranieri[a], G. Selvaggi[a,b], A. Sharma[a], L. Silvestris[a,14], R. Venditti[a], P. Verwilligen[a]

INFN Sezione di Bologna [a], Università di Bologna [b], Bologna, Italy

G. Abbiendi[a], C. Battilana[a,b], D. Bonacorsi[a,b], S. Braibant-Giacomelli[a,b], R. Campanini[a,b], P. Capiluppi[a,b], A. Castro[a,b], F.R. Cavallo[a], S.S. Chhibra[a], G. Codispoti[a,b], M. Cuffiani[a,b], G.M. Dallavalle[a], F. Fabbri[a], A. Fanfani[a,b], D. Fasanella[a,b], P. Giacomelli[a], C. Grandi[a], L. Guiducci[a,b], S. Marcellini[a], G. Masetti[a], A. Montanari[a], F.L. Navarria[a,b], A. Perrotta[a], A.M. Rossi[a,b], T. Rovelli[a,b], G.P. Siroli[a,b], N. Tosi[a]

INFN Sezione di Catania [a], Università di Catania [b], Catania, Italy

S. Albergo[a,b], S. Costa[a,b], A. Di Mattia[a], F. Giordano[a,b], R. Potenza[a,b], A. Tricomi[a,b], C. Tuve[a,b]

INFN Sezione di Firenze [a], Università di Firenze [b], Firenze, Italy

G. Barbagli[a], K. Chatterjee[a,b], V. Ciulli[a,b], C. Civinini[a], R. D'Alessandro[a,b], E. Focardi[a,b], P. Lenzi[a,b], M. Meschini[a], S. Paoletti[a], L. Russo[a,28], G. Sguazzoni[a], D. Strom[a], L. Viliani[a,b,14]

INFN Laboratori Nazionali di Frascati, Frascati, Italy
L. Benussi, S. Bianco, F. Fabbri, D. Piccolo, F. Primavera[14]

INFN Sezione di Genova [a], Università di Genova [b], Genova, Italy
V. Calvelli[a,b], F. Ferro[a], E. Robutti[a], S. Tosi[a,b]

INFN Sezione di Milano-Bicocca [a], Università di Milano-Bicocca [b], Milano, Italy
A. Benaglia[a], L. Brianza[a,b], F. Brivio[a,b], V. Ciriolo[a,b], M.E. Dinardo[a,b], S. Fiorendi[a,b], S. Gennai[a], A. Ghezzi[a,b], P. Govoni[a,b], M. Malberti[a,b], S. Malvezzi[a], R.A. Manzoni[a,b], D. Menasce[a], L. Moroni[a], M. Paganoni[a,b], K. Pauwels[a,b], D. Pedrini[a], S. Pigazzini[a,b,29], S. Ragazzi[a,b], T. Tabarelli de Fatis[a,b]

INFN Sezione di Napoli [a], Università di Napoli 'Federico II' [b], Napoli, Italy, Università della Basilicata [c], Potenza, Italy, Università G. Marconi [d], Roma, Italy
S. Buontempo[a], N. Cavallo[a,c], S. Di Guida[a,d,14], F. Fabozzi[a,c], F. Fienga[a,b], A.O.M. Iorio[a,b], W.A. Khan[a], L. Lista[a], S. Meola[a,d,14], P. Paolucci[a,14], C. Sciacca[a,b], F. Thyssen[a]

INFN Sezione di Padova [a], Università di Padova [b], Padova, Italy, Università di Trento [c], Trento, Italy
P. Azzi[a,14], N. Bacchetta[a], L. Benato[a,b], D. Bisello[a,b], A. Boletti[a,b], R. Carlin[a,b], A. Carvalho Antunes De Oliveira[a,b], P. Checchia[a], M. Dall'Osso[a,b], P. De Castro Manzano[a], T. Dorigo[a], U. Dosselli[a], F. Gasparini[a,b], A. Gozzelino[a], S. Lacaprara[a], P. Lujan, M. Margoni[a,b], A.T. Meneguzzo[a,b], N. Pozzobon[a,b], P. Ronchese[a,b], R. Rossin[a,b], F. Simonetto[a,b], S. Ventura[a], M. Zanetti[a,b], P. Zotto[a,b], G. Zumerle[a,b]

INFN Sezione di Pavia [a], Università di Pavia [b], Pavia, Italy
A. Braghieri[a], A. Magnani[a,b], P. Montagna[a,b], S.P. Ratti[a,b], V. Re[a], M. Ressegotti, C. Riccardi[a,b], P. Salvini[a], I. Vai[a,b], P. Vitulo[a,b]

INFN Sezione di Perugia [a], Università di Perugia [b], Perugia, Italy
L. Alunni Solestizi[a,b], M. Biasini[a,b], G.M. Bilei[a], C. Cecchi[a,b], D. Ciangottini[a,b], L. Fanò[a,b], P. Lariccia[a,b], R. Leonardi[a,b], E. Manoni[a], G. Mantovani[a,b], V. Mariani[a,b], M. Menichelli[a], A. Rossi[a,b], A. Santocchia[a,b], D. Spiga[a]

INFN Sezione di Pisa [a], Università di Pisa [b], Scuola Normale Superiore di Pisa [c], Pisa, Italy
K. Androsov[a], P. Azzurri[a,14], G. Bagliesi[a], T. Boccali[a], L. Borrello, R. Castaldi[a], M.A. Ciocci[a,b], R. Dell'Orso[a], G. Fedi[a], L. Giannini[a,c], A. Giassi[a], M.T. Grippo[a,28], F. Ligabue[a,c], T. Lomtadze[a], E. Manca[a,c], G. Mandorli[a,c], L. Martini[a,b], A. Messineo[a,b], F. Palla[a], A. Rizzi[a,b], A. Savoy-Navarro[a,30], P. Spagnolo[a], R. Tenchini[a], G. Tonelli[a,b], A. Venturi[a], P.G. Verdini[a]

INFN Sezione di Roma [a], Sapienza Università di Roma [b], Rome, Italy
L. Barone[a,b], F. Cavallari[a], M. Cipriani[a,b], N. Daci[a], D. Del Re[a,b,14], E. Di Marco[a,b], M. Diemoz[a], S. Gelli[a,b], E. Longo[a,b], F. Margaroli[a,b], B. Marzocchi[a,b],

P. Meridiani[a], G. Organtini[a,b], R. Paramatti[a,b], F. Preiato[a,b], S. Rahatlou[a,b], C. Rovelli[a], F. Santanastasio[a,b]

INFN Sezione di Torino [a], Università di Torino [b], Torino, Italy, Università del Piemonte Orientale [c], Novara, Italy

N. Amapane[a,b], R. Arcidiacono[a,c], S. Argiro[a,b], M. Arneodo[a,c], N. Bartosik[a], R. Bellan[a,b], C. Biino[a], N. Cartiglia[a], F. Cenna[a,b], M. Costa[a,b], R. Covarelli[a,b], A. Degano[a,b], N. Demaria[a], B. Kiani[a,b], C. Mariotti[a], S. Maselli[a], E. Migliore[a,b], V. Monaco[a,b], E. Monteil[a,b], M. Monteno[a], M.M. Obertino[a,b], L. Pacher[a,b], N. Pastrone[a], M. Pelliccioni[a], G.L. Pinna Angioni[a,b], F. Ravera[a,b], A. Romero[a,b], M. Ruspa[a,c], R. Sacchi[a,b], K. Shchelina[a,b], V. Sola[a], A. Solano[a,b], A. Staiano[a], P. Traczyk[a,b]

INFN Sezione di Trieste [a], Università di Trieste [b], Trieste, Italy

S. Belforte[a], M. Casarsa[a], F. Cossutti[a], G. Della Ricca[a,b], A. Zanetti[a]

Kyungpook National University, Daegu, Korea

D.H. Kim, G.N. Kim, M.S. Kim, J. Lee, S. Lee, S.W. Lee, C.S. Moon, Y.D. Oh, S. Sekmen, D.C. Son, Y.C. Yang

Chonbuk National University, Jeonju, Korea

A. Lee

Chonnam National University, Institute for Universe and Elementary Particles, Kwangju, Korea

H. Kim, D.H. Moon, G. Oh

Hanyang University, Seoul, Korea

J.A. Brochero Cifuentes, J. Goh, T.J. Kim

Korea University, Seoul, Korea

S. Cho, S. Choi, Y. Go, D. Gyun, S. Ha, B. Hong, Y. Jo, Y. Kim, K. Lee, K.S. Lee, S. Lee, J. Lim, S.K. Park, Y. Roh

Seoul National University, Seoul, Korea

J. Almond, J. Kim, J.S. Kim, H. Lee, K. Lee, K. Nam, S.B. Oh, B.C. Radburn-Smith, S.h. Seo, U.K. Yang, H.D. Yoo, G.B. Yu

University of Seoul, Seoul, Korea

M. Choi, H. Kim, J.H. Kim, J.S.H. Lee, I.C. Park

Sungkyunkwan University, Suwon, Korea

Y. Choi, C. Hwang, J. Lee, I. Yu

Vilnius University, Vilnius, Lithuania

V. Dudenas, A. Juodagalvis, J. Vaitkus

National Centre for Particle Physics, Universiti Malaya, Kuala Lumpur, Malaysia

I. Ahmed, Z.A. Ibrahim, M.A.B. Md Ali[31], F. Mohamad Idris[32], W.A.T. Wan Abdullah, M.N. Yusli, Z. Zolkapli

Centro de Investigacion y de Estudios Avanzados del IPN, Mexico City, Mexico

Reyes-Almanza, R, Ramirez-Sanchez, G., Duran-Osuna, M. C., H. Castilla-Valdez, E. De La Cruz-Burelo, I. Heredia-De La Cruz[33], Rabadan-Trejo, R. I., R. Lopez-Fernandez, J. Mejia Guisao, A. Sanchez-Hernandez

Universidad Iberoamericana, Mexico City, Mexico

S. Carrillo Moreno, C. Oropeza Barrera, F. Vazquez Valencia

Benemerita Universidad Autonoma de Puebla, Puebla, Mexico

I. Pedraza, H.A. Salazar Ibarguen, C. Uribe Estrada

Universidad Autónoma de San Luis Potosí, San Luis Potosí, Mexico

A. Morelos Pineda

University of Auckland, Auckland, New Zealand

D. Krofcheck

University of Canterbury, Christchurch, New Zealand

P.H. Butler

National Centre for Physics, Quaid-I-Azam University, Islamabad, Pakistan

A. Ahmad, M. Ahmad, Q. Hassan, H.R. Hoorani, S. Qazi, A. Saddique, M.A. Shah, M. Waqas

National Centre for Nuclear Research, Swierk, Poland

H. Bialkowska, M. Bluj, B. Boimska, T. Frueboes, M. Górski, M. Kazana, K. Nawrocki, M. Szleper, P. Zalewski

Institute of Experimental Physics, Faculty of Physics, University of Warsaw, Warsaw, Poland

K. Bunkowski, A. Byszuk[34], K. Doroba, A. Kalinowski, M. Konecki, J. Krolikowski, M. Misiura, M. Olszewski, A. Pyskir, M. Walczak

Laboratório de Instrumentação e Física Experimental de Partículas, Lisboa, Portugal

P. Bargassa, C. Beirão Da Cruz E Silva, A. Di Francesco, P. Faccioli, B. Galinhas, M. Gallinaro, J. Hollar, N. Leonardo, L. Lloret Iglesias, M.V. Nemallapudi, J. Seixas, G. Strong, O. Toldaiev, D. Vadruccio, J. Varela

Joint Institute for Nuclear Research, Dubna, Russia

I. Golutvin, V. Karjavin, I. Kashunin, V. Korenkov, G. Kozlov, A. Lanev, A. Malakhov, V. Matveev[35,36], V.V. Mitsyn, V. Palichik, V. Perelygin, S. Shmatov, V. Smirnov, V. Trofimov, N. Voytishin, B.S. Yuldashev[37], A. Zarubin, V. Zhiltsov

Petersburg Nuclear Physics Institute, Gatchina (St. Petersburg), Russia

Y. Ivanov, V. Kim[38], E. Kuznetsova[39], P. Levchenko, V. Murzin, V. Oreshkin, I. Smirnov, V. Sulimov, L. Uvarov, S. Vavilov, A. Vorobyev

Institute for Nuclear Research, Moscow, Russia

Yu. Andreev, A. Dermenev, S. Gninenko, N. Golubev, A. Karneyeu, M. Kirsanov, N. Krasnikov, A. Pashenkov, D. Tlisov, A. Toropin

Institute for Theoretical and Experimental Physics, Moscow, Russia

V. Epshteyn, V. Gavrilov, N. Lychkovskaya, V. Popov, I. Pozdnyakov, G. Safronov, A. Spiridonov, A. Stepennov, M. Toms, E. Vlasov, A. Zhokin

Moscow Institute of Physics and Technology, Moscow, Russia

T. Aushev, A. Bylinkin[36]

National Research Nuclear University 'Moscow Engineering Physics Institute' (MEPhI), Moscow, Russia

M. Chadeeva[40], P. Parygin, D. Philippov, S. Polikarpov, E. Popova, V. Rusinov

P.N. Lebedev Physical Institute, Moscow, Russia

V. Andreev, M. Azarkin[36], I. Dremin[36], M. Kirakosyan[36], A. Terkulov

Skobeltsyn Institute of Nuclear Physics, Lomonosov Moscow State University, Moscow, Russia

A. Baskakov, A. Belyaev, E. Boos, V. Bunichev, M. Dubinin[41], L. Dudko, A. Gribushin, V. Klyukhin, N. Korneeva, I. Lokhtin, I. Miagkov, S. Obraztsov, M. Perfilov, V. Savrin, P. Volkov

Novosibirsk State University (NSU), Novosibirsk, Russia

V. Blinov[42], Y.Skovpen[42], D. Shtol[42]

State Research Center of Russian Federation, Institute for High Energy Physics, Protvino, Russia

I. Azhgirey, I. Bayshev, S. Bitioukov, D. Elumakhov, V. Kachanov, A. Kalinin, D. Konstantinov, V. Krychkine, V. Petrov, R. Ryutin, A. Sobol, S. Troshin, N. Tyurin, A. Uzunian, A. Volkov

University of Belgrade, Faculty of Physics and Vinca Institute of Nuclear Sciences, Belgrade, Serbia

P. Adzic[43], P. Cirkovic, D. Devetak, M. Dordevic, J. Milosevic, V. Rekovic

Centro de Investigaciones Energéticas Medioambientales y Tecnológicas (CIEMAT), Madrid, Spain

J. Alcaraz Maestre, M. Barrio Luna, M. Cerrada, N. Colino, B. De La Cruz, A. Delgado Peris, A. Escalante Del Valle, C. Fernandez Bedoya, J.P. Fernández Ramos, J. Flix, M.C. Fouz, P. Garcia-Abia, O. Gonzalez Lopez, S. Goy Lopez, J.M. Hernandez, M.I. Josa, A. Pérez-Calero Yzquierdo, J. Puerta Pelayo, A. Quintario Olmeda, I. Redondo, L. Romero, M.S. Soares, A. Álvarez Fernández

Universidad Autónoma de Madrid, Madrid, Spain

C. Albajar, J.F. de Trocóniz, M. Missiroli, D. Moran

Universidad de Oviedo, Oviedo, Spain

J. Cuevas, C. Erice, J. Fernandez Menendez, I. Gonzalez Caballero, J.R. González Fernández, E. Palencia Cortezon, S. Sanchez Cruz, P. Vischia, J.M. Vizan Garcia

Instituto de Física de Cantabria (IFCA), CSIC-Universidad de Cantabria, Santander, Spain

I.J. Cabrillo, A. Calderon, B. Chazin Quero, E. Curras, J. Duarte Campderros, M. Fernandez, J. Garcia-Ferrero, G. Gomez, A. Lopez Virto, J. Marco, C. Martinez Rivero, P. Martinez Ruiz del Arbol, F. Matorras, J. Piedra Gomez, T. Rodrigo, A. Ruiz-Jimeno, L. Scodellaro, N. Trevisani, I. Vila, R. Vilar Cortabitarte

CERN, European Organization for Nuclear Research, Geneva, Switzerland

D. Abbaneo, E. Auffray, P. Baillon, A.H. Ball, D. Barney, M. Bianco, P. Bloch, A. Bocci, C. Botta, T. Camporesi, R. Castello, M. Cepeda, G. Cerminara, E. Chapon, Y. Chen, D. d'Enterria, A. Dabrowski, V. Daponte, A. David, M. De Gruttola, A. De Roeck, M. Dobson, B. Dorney, T. du Pree, M. Dünser, N. Dupont, A. Elliott-Peisert, P. Everaerts, F. Fallavollita, G. Franzoni, J. Fulcher, W. Funk, D. Gigi, K. Gill, F. Glege, D. Gulhan, P. Harris, J. Hegeman, V. Innocente, P. Janot, O. Karacheban[17], J. Kieseler, H. Kirschenmann, V. Knünz, A. Kornmayer[14], M.J. Kortelainen, M. Krammer[1], C. Lange, P. Lecoq, C. Lourenço, M.T. Lucchini, L. Malgeri, M. Mannelli, A. Martelli, F. Meijers, J.A. Merlin, S. Mersi, E. Meschi, P. Milenovic[44], F. Moortgat, M. Mulders, H. Neugebauer, S. Orfanelli, L. Orsini, L. Pape, E. Perez, M. Peruzzi, A. Petrilli, G. Petrucciani, A. Pfeiffer, M. Pierini, A. Racz, T. Reis, G. Rolandi[45], M. Rovere, H. Sakulin, C. Schäfer, C. Schwick, M. Seidel, M. Selvaggi, A. Sharma, P. Silva, P. Sphicas[46], A. Stakia, J. Steggemann, M. Stoye, M. Tosi, D. Treille, A. Triossi, A. Tsirou, V. Veckalns[47], M. Verweij, W.D. Zeuner

Paul Scherrer Institut, Villigen, Switzerland

W. Bertl[†], L. Caminada[48], K. Deiters, W. Erdmann, R. Horisberger, Q. Ingram, H.C. Kaestli, D. Kotlinski, U. Langenegger, T. Rohe, S.A. Wiederkehr

ETH Zurich — Institute for Particle Physics and Astrophysics (IPA), Zurich, Switzerland

F. Bachmair, L. Bäni, P. Berger, L. Bianchini, B. Casal, G. Dissertori, M. Dittmar, M. Donegà, C. Grab, C. Heidegger, D. Hits, J. Hoss, G. Kasieczka, T. Klijnsma, W. Lustermann, B. Mangano, M. Marionneau, M.T. Meinhard, D. Meister, F. Micheli, P. Musella, F. Nessi-Tedaldi, F. Pandolfi, J. Pata, F. Pauss, G. Perrin, L. Perrozzi, M. Quittnat, M. Reichmann, M. Schönenberger, L. Shchutska, V.R. Tavolaro, K. Theofilatos, M.L. Vesterbacka Olsson, R. Wallny, D.H. Zhu

Universität Zürich, Zurich, Switzerland

T.K. Aarrestad, C. Amsler[49], M.F. Canelli, A. De Cosa, R. Del Burgo, S. Donato, C. Galloni, T. Hreus, B. Kilminster, J. Ngadiuba, D. Pinna, G. Rauco, P. Robmann, D. Salerno, C. Seitz, Y. Takahashi, A. Zucchetta

National Central University, Chung-Li, Taiwan

V. Candelise, T.H. Doan, Sh. Jain, R. Khurana, C.M. Kuo, W. Lin, A. Pozdnyakov, S.S. Yu

National Taiwan University (NTU), Taipei, Taiwan

Arun Kumar, P. Chang, Y. Chao, K.F. Chen, P.H. Chen, F. Fiori, W.-S. Hou, Y. Hsiung, Y.F. Liu, R.-S. Lu, E. Paganis, A. Psallidas, A. Steen, J.f. Tsai

Chulalongkorn University, Faculty of Science, Department of Physics, Bangkok, Thailand

B. Asavapibhop, K. Kovitanggoon, G. Singh, N. Srimanobhas

Çukurova University, Physics Department, Science and Art Faculty, Adana, Turkey

M.N. Bakirci[50], F. Boran, S. Damarseckin, Z.S. Demiroglu, C. Dozen, S. Girgis, G. Gokbulut, Y. Guler, I. Hos[51], E.E. Kangal[52], O. Kara, A. Kayis Topaksu, U. Kiminsu, M. Oglakci, G. Onengut[53], K. Ozdemir[54], S. Ozturk[50], A. Polatoz, H. Topakli[50], S. Turkcapar, I.S. Zorbakir, C. Zorbilmez

Middle East Technical University, Physics Department, Ankara, Turkey

B. Bilin, G. Karapinar[55], K. Ocalan[56], M. Yalvac, M. Zeyrek

Bogazici University, Istanbul, Turkey

E. Gülmez, M. Kaya[57], O. Kaya[58], S. Tekten, E.A. Yetkin[59]

Istanbul Technical University, Istanbul, Turkey

M.N. Agaras, S. Atay, A. Cakir, K. Cankocak

Institute for Scintillation Materials of National Academy of Science of Ukraine, Kharkov, Ukraine

B. Grynyov

National Scientific Center, Kharkov Institute of Physics and Technology, Kharkov, Ukraine

L. Levchuk, P. Sorokin

University of Bristol, Bristol, United Kingdom

R. Aggleton, F. Ball, L. Beck, J.J. Brooke, D. Burns, E. Clement, D. Cussans, O. Davignon, H. Flacher, J. Goldstein, M. Grimes, G.P. Heath, H.F. Heath, J. Jacob, L. Kreczko, C. Lucas, D.M. Newbold[60], S. Paramesvaran, A. Poll, T. Sakuma, S. Seif El Nasr-storey, D. Smith, V.J. Smith

Rutherford Appleton Laboratory, Didcot, United Kingdom

K.W. Bell, A. Belyaev[61], C. Brew, R.M. Brown, L. Calligaris, D. Cieri, D.J.A. Cockerill, J.A. Coughlan, K. Harder, S. Harper, E. Olaiya, D. Petyt, C.H. Shepherd-Themistocleous, A. Thea, I.R. Tomalin, T. Williams

Imperial College, London, United Kingdom

G. Auzinger, R. Bainbridge, S. Breeze, O. Buchmuller, A. Bundock, S. Casasso, M. Citron, D. Colling, L. Corpe, P. Dauncey, G. Davies, A. De Wit, M. Della Negra, R. Di Maria, A. Elwood, Y. Haddad, G. Hall, G. Iles, T. James, R. Lane, C. Laner, L. Lyons, A.-M. Magnan, S. Malik, L. Mastrolorenzo, T. Matsushita, J. Nash, A. Nikitenko[6],

V. Palladino, M. Pesaresi, D.M. Raymond, A. Richards, A. Rose, E. Scott, C. Seez, A. Shtipliyski, S. Summers, A. Tapper, K. Uchida, M. Vazquez Acosta[62], T. Virdee[14], N. Wardle, D. Winterbottom, J. Wright, S.C. Zenz

Brunel University, Uxbridge, United Kingdom

J.E. Cole, P.R. Hobson, A. Khan, P. Kyberd, I.D. Reid, P. Symonds, L. Teodorescu, M. Turner

Baylor University, Waco, U.S.A.

A. Borzou, K. Call, J. Dittmann, K. Hatakeyama, H. Liu, N. Pastika, C. Smith

Catholic University of America, Washington DC, U.S.A.

R. Bartek, A. Dominguez

The University of Alabama, Tuscaloosa, U.S.A.

A. Buccilli, S.I. Cooper, C. Henderson, P. Rumerio, C. West

Boston University, Boston, U.S.A.

D. Arcaro, A. Avetisyan, T. Bose, D. Gastler, D. Rankin, C. Richardson, J. Rohlf, L. Sulak, D. Zou

Brown University, Providence, U.S.A.

G. Benelli, D. Cutts, A. Garabedian, J. Hakala, U. Heintz, J.M. Hogan, K.H.M. Kwok, E. Laird, G. Landsberg, Z. Mao, M. Narain, J. Pazzini, S. Piperov, S. Sagir, R. Syarif, D. Yu

University of California, Davis, Davis, U.S.A.

R. Band, C. Brainerd, R. Breedon, D. Burns, M. Calderon De La Barca Sanchez, M. Chertok, J. Conway, R. Conway, P.T. Cox, R. Erbacher, C. Flores, G. Funk, M. Gardner, W. Ko, R. Lander, C. Mclean, M. Mulhearn, D. Pellett, J. Pilot, S. Shalhout, M. Shi, J. Smith, M. Squires, D. Stolp, K. Tos, M. Tripathi, Z. Wang

University of California, Los Angeles, U.S.A.

M. Bachtis, C. Bravo, R. Cousins, A. Dasgupta, A. Florent, J. Hauser, M. Ignatenko, N. Mccoll, D. Saltzberg, C. Schnaible, V. Valuev

University of California, Riverside, Riverside, U.S.A.

E. Bouvier, K. Burt, R. Clare, J. Ellison, J.W. Gary, S.M.A. Ghiasi Shirazi, G. Hanson, J. Heilman, P. Jandir, E. Kennedy, F. Lacroix, O.R. Long, M. Olmedo Negrete, M.I. Paneva, A. Shrinivas, W. Si, L. Wang, H. Wei, S. Wimpenny, B. R. Yates

University of California, San Diego, La Jolla, U.S.A.

J.G. Branson, S. Cittolin, M. Derdzinski, R. Gerosa, B. Hashemi, A. Holzner, D. Klein, G. Kole, V. Krutelyov, J. Letts, I. Macneill, M. Masciovecchio, D. Olivito, S. Padhi, M. Pieri, M. Sani, V. Sharma, S. Simon, M. Tadel, A. Vartak, S. Wasserbaech[63], J. Wood, F. Würthwein, A. Yagil, G. Zevi Della Porta

University of California, Santa Barbara — Department of Physics, Santa Barbara, U.S.A.

N. Amin, R. Bhandari, J. Bradmiller-Feld, C. Campagnari, A. Dishaw, V. Dutta, M. Franco Sevilla, C. George, F. Golf, L. Gouskos, J. Gran, R. Heller, J. Incandela, S.D. Mullin, A. Ovcharova, H. Qu, J. Richman, D. Stuart, I. Suarez, J. Yoo

California Institute of Technology, Pasadena, U.S.A.

D. Anderson, J. Bendavid, A. Bornheim, J.M. Lawhorn, H.B. Newman, T. Nguyen, C. Pena, M. Spiropulu, J.R. Vlimant, S. Xie, Z. Zhang, R.Y. Zhu

Carnegie Mellon University, Pittsburgh, U.S.A.

M.B. Andrews, T. Ferguson, T. Mudholkar, M. Paulini, J. Russ, M. Sun, H. Vogel, I. Vorobiev, M. Weinberg

University of Colorado Boulder, Boulder, U.S.A.

J.P. Cumalat, W.T. Ford, F. Jensen, A. Johnson, M. Krohn, S. Leontsinis, T. Mulholland, K. Stenson, S.R. Wagner

Cornell University, Ithaca, U.S.A.

J. Alexander, J. Chaves, J. Chu, S. Dittmer, K. Mcdermott, N. Mirman, J.R. Patterson, A. Rinkevicius, A. Ryd, L. Skinnari, L. Soffi, S.M. Tan, Z. Tao, J. Thom, J. Tucker, P. Wittich, M. Zientek

Fermi National Accelerator Laboratory, Batavia, U.S.A.

S. Abdullin, M. Albrow, G. Apollinari, A. Apresyan, A. Apyan, S. Banerjee, L.A.T. Bauerdick, A. Beretvas, J. Berryhill, P.C. Bhat, G. Bolla[†], K. Burkett, J.N. Butler, A. Canepa, G.B. Cerati, H.W.K. Cheung, F. Chlebana, M. Cremonesi, J. Duarte, V.D. Elvira, J. Freeman, Z. Gecse, E. Gottschalk, L. Gray, D. Green, S. Grünendahl, O. Gutsche, R.M. Harris, S. Hasegawa, J. Hirschauer, Z. Hu, B. Jayatilaka, S. Jindariani, M. Johnson, U. Joshi, B. Klima, B. Kreis, S. Lammel, D. Lincoln, R. Lipton, M. Liu, T. Liu, R. Lopes De Sá, J. Lykken, K. Maeshima, N. Magini, J.M. Marraffino, S. Maruyama, D. Mason, P. McBride, P. Merkel, S. Mrenna, S. Nahn, V. O'Dell, K. Pedro, O. Prokofyev, G. Rakness, L. Ristori, B. Schneider, E. Sexton-Kennedy, A. Soha, W.J. Spalding, L. Spiegel, S. Stoynev, J. Strait, N. Strobbe, L. Taylor, S. Tkaczyk, N.V. Tran, L. Uplegger, E.W. Vaandering, C. Vernieri, M. Verzocchi, R. Vidal, M. Wang, H.A. Weber, A. Whitbeck

University of Florida, Gainesville, U.S.A.

D. Acosta, P. Avery, P. Bortignon, D. Bourilkov, A. Brinkerhoff, A. Carnes, M. Carver, D. Curry, R.D. Field, I.K. Furic, J. Konigsberg, A. Korytov, K. Kotov, P. Ma, K. Matchev, H. Mei, G. Mitselmakher, D. Rank, D. Sperka, N. Terentyev, L. Thomas, J. Wang, S. Wang, J. Yelton

Florida International University, Miami, U.S.A.

Y.R. Joshi, S. Linn, P. Markowitz, J.L. Rodriguez

Florida State University, Tallahassee, U.S.A.

A. Ackert, T. Adams, A. Askew, S. Hagopian, V. Hagopian, K.F. Johnson, T. Kolberg, G. Martinez, T. Perry, H. Prosper, A. Saha, A. Santra, V. Sharma, R. Yohay

Florida Institute of Technology, Melbourne, U.S.A.

M.M. Baarmand, V. Bhopatkar, S. Colafranceschi, M. Hohlmann, D. Noonan, T. Roy, F. Yumiceva

University of Illinois at Chicago (UIC), Chicago, U.S.A.

M.R. Adams, L. Apanasevich, D. Berry, R.R. Betts, R. Cavanaugh, X. Chen, O. Evdokimov, C.E. Gerber, D.A. Hangal, D.J. Hofman, K. Jung, J. Kamin, I.D. Sandoval Gonzalez, M.B. Tonjes, H. Trauger, N. Varelas, H. Wang, Z. Wu, J. Zhang

The University of Iowa, Iowa City, U.S.A.

B. Bilki[64], W. Clarida, K. Dilsiz[65], S. Durgut, R.P. Gandrajula, M. Haytmyradov, V. Khristenko, J.-P. Merlo, H. Mermerkaya[66], A. Mestvirishvili, A. Moeller, J. Nachtman, H. Ogul[67], Y. Onel, F. Ozok[68], A. Penzo, C. Snyder, E. Tiras, J. Wetzel, K. Yi

Johns Hopkins University, Baltimore, U.S.A.

B. Blumenfeld, A. Cocoros, N. Eminizer, D. Fehling, L. Feng, A.V. Gritsan, P. Maksimovic, J. Roskes, U. Sarica, M. Swartz, M. Xiao, C. You

The University of Kansas, Lawrence, U.S.A.

A. Al-bataineh, P. Baringer, A. Bean, S. Boren, J. Bowen, J. Castle, S. Khalil, A. Kropivnitskaya, D. Majumder, W. Mcbrayer, M. Murray, C. Royon, S. Sanders, E. Schmitz, J.D. Tapia Takaki, Q. Wang

Kansas State University, Manhattan, U.S.A.

A. Ivanov, K. Kaadze, Y. Maravin, A. Mohammadi, L.K. Saini, N. Skhirtladze, S. Toda

Lawrence Livermore National Laboratory, Livermore, U.S.A.

F. Rebassoo, D. Wright

University of Maryland, College Park, U.S.A.

C. Anelli, A. Baden, O. Baron, A. Belloni, B. Calvert, S.C. Eno, C. Ferraioli, N.J. Hadley, S. Jabeen, G.Y. Jeng, R.G. Kellogg, J. Kunkle, A.C. Mignerey, F. Ricci-Tam, Y.H. Shin, A. Skuja, S.C. Tonwar

Massachusetts Institute of Technology, Cambridge, U.S.A.

D. Abercrombie, B. Allen, V. Azzolini, R. Barbieri, A. Baty, R. Bi, S. Brandt, W. Busza, I.A. Cali, M. D'Alfonso, Z. Demiragli, G. Gomez Ceballos, M. Goncharov, D. Hsu, Y. Iiyama, G.M. Innocenti, M. Klute, D. Kovalskyi, Y.S. Lai, Y.-J. Lee, A. Levin, P.D. Luckey, B. Maier, A.C. Marini, C. Mcginn, C. Mironov, S. Narayanan, X. Niu, C. Paus, C. Roland, G. Roland, J. Salfeld-Nebgen, G.S.F. Stephans, K. Tatar, D. Velicanu, J. Wang, T.W. Wang, B. Wyslouch

University of Minnesota, Minneapolis, U.S.A.

A.C. Benvenuti, R.M. Chatterjee, A. Evans, P. Hansen, S. Kalafut, Y. Kubota, Z. Lesko, J. Mans, S. Nourbakhsh, N. Ruckstuhl, R. Rusack, J. Turkewitz

University of Mississippi, Oxford, U.S.A.

J.G. Acosta, S. Oliveros

University of Nebraska-Lincoln, Lincoln, U.S.A.
E. Avdeeva, K. Bloom, D.R. Claes, C. Fangmeier, R. Gonzalez Suarez, R. Kamalieddin, I. Kravchenko, J. Monroy, J.E. Siado, G.R. Snow, B. Stieger

State University of New York at Buffalo, Buffalo, U.S.A.
M. Alyari, J. Dolen, A. Godshalk, C. Harrington, I. Iashvili, D. Nguyen, A. Parker, S. Rappoccio, B. Roozbahani

Northeastern University, Boston, U.S.A.
G. Alverson, E. Barberis, A. Hortiangtham, A. Massironi, D.M. Morse, D. Nash, T. Orimoto, R. Teixeira De Lima, D. Trocino, D. Wood

Northwestern University, Evanston, U.S.A.
S. Bhattacharya, O. Charaf, K.A. Hahn, N. Mucia, N. Odell, B. Pollack, M.H. Schmitt, K. Sung, M. Trovato, M. Velasco

University of Notre Dame, Notre Dame, U.S.A.
N. Dev, M. Hildreth, K. Hurtado Anampa, C. Jessop, D.J. Karmgard, N. Kellams, K. Lannon, N. Loukas, N. Marinelli, F. Meng, C. Mueller, Y. Musienko[35], M. Planer, A. Reinsvold, R. Ruchti, G. Smith, S. Taroni, M. Wayne, M. Wolf, A. Woodard

The Ohio State University, Columbus, U.S.A.
J. Alimena, L. Antonelli, B. Bylsma, L.S. Durkin, S. Flowers, B. Francis, A. Hart, C. Hill, W. Ji, B. Liu, W. Luo, D. Puigh, B.L. Winer, H.W. Wulsin

Princeton University, Princeton, U.S.A.
S. Cooperstein, O. Driga, P. Elmer, J. Hardenbrook, P. Hebda, S. Higginbotham, D. Lange, J. Luo, D. Marlow, K. Mei, I. Ojalvo, J. Olsen, C. Palmer, P. Piroué, D. Stickland, C. Tully

University of Puerto Rico, Mayaguez, U.S.A.
S. Malik, S. Norberg

Purdue University, West Lafayette, U.S.A.
A. Barker, V.E. Barnes, S. Das, S. Folgueras, L. Gutay, M.K. Jha, M. Jones, A.W. Jung, A. Khatiwada, D.H. Miller, N. Neumeister, C.C. Peng, J.F. Schulte, J. Sun, F. Wang, W. Xie

Purdue University Northwest, Hammond, U.S.A.
T. Cheng, N. Parashar, J. Stupak

Rice University, Houston, U.S.A.
A. Adair, B. Akgun, Z. Chen, K.M. Ecklund, F.J.M. Geurts, M. Guilbaud, W. Li, B. Michlin, M. Northup, B.P. Padley, J. Roberts, J. Rorie, Z. Tu, J. Zabel

University of Rochester, Rochester, U.S.A.
A. Bodek, P. de Barbaro, R. Demina, Y.t. Duh, T. Ferbel, M. Galanti, A. Garcia-Bellido, J. Han, O. Hindrichs, A. Khukhunaishvili, K.H. Lo, P. Tan, M. Verzetti

The Rockefeller University, New York, U.S.A.
R. Ciesielski, K. Goulianos, C. Mesropian

Rutgers, The State University of New Jersey, Piscataway, U.S.A.
A. Agapitos, J.P. Chou, Y. Gershtein, T.A. Gómez Espinosa, E. Halkiadakis, M. Heindl, E. Hughes, S. Kaplan, R. Kunnawalkam Elayavalli, S. Kyriacou, A. Lath, R. Montalvo, K. Nash, M. Osherson, H. Saka, S. Salur, S. Schnetzer, D. Sheffield, S. Somalwar, R. Stone, S. Thomas, P. Thomassen, M. Walker

University of Tennessee, Knoxville, U.S.A.
A.G. Delannoy, M. Foerster, J. Heideman, G. Riley, K. Rose, S. Spanier, K. Thapa

Texas A&M University, College Station, U.S.A.
O. Bouhali[69], A. Castaneda Hernandez[69], A. Celik, M. Dalchenko, M. De Mattia, A. Delgado, S. Dildick, R. Eusebi, J. Gilmore, T. Huang, T. Kamon[70], R. Mueller, Y. Pakhotin, R. Patel, A. Perloff, L. Perniè, D. Rathjens, A. Safonov, A. Tatarinov, K.A. Ulmer

Texas Tech University, Lubbock, U.S.A.
N. Akchurin, J. Damgov, F. De Guio, P.R. Dudero, J. Faulkner, E. Gurpinar, S. Kunori, K. Lamichhane, S.W. Lee, T. Libeiro, T. Peltola, S. Undleeb, I. Volobouev, Z. Wang

Vanderbilt University, Nashville, U.S.A.
S. Greene, A. Gurrola, R. Janjam, W. Johns, C. Maguire, A. Melo, H. Ni, P. Sheldon, S. Tuo, J. Velkovska, Q. Xu

University of Virginia, Charlottesville, U.S.A.
M.W. Arenton, P. Barria, B. Cox, R. Hirosky, M. Joyce, A. Ledovskoy, H. Li, C. Neu, T. Sinthuprasith, Y. Wang, E. Wolfe, F. Xia

Wayne State University, Detroit, U.S.A.
R. Harr, P.E. Karchin, J. Sturdy, S. Zaleski

University of Wisconsin — Madison, Madison, WI, U.S.A.
M. Brodski, J. Buchanan, C. Caillol, S. Dasu, L. Dodd, S. Duric, B. Gomber, M. Grothe, M. Herndon, A. Hervé, U. Hussain, P. Klabbers, A. Lanaro, A. Levine, K. Long, R. Loveless, G.A. Pierro, G. Polese, T. Ruggles, A. Savin, N. Smith, W.H. Smith, D. Taylor, N. Woods

†: Deceased
1: Also at Vienna University of Technology, Vienna, Austria
2: Also at State Key Laboratory of Nuclear Physics and Technology, Peking University, Beijing, China
3: Also at Universidade Estadual de Campinas, Campinas, Brazil
4: Also at Universidade Federal de Pelotas, Pelotas, Brazil
5: Also at Université Libre de Bruxelles, Bruxelles, Belgium
6: Also at Institute for Theoretical and Experimental Physics, Moscow, Russia
7: Also at Joint Institute for Nuclear Research, Dubna, Russia
8: Also at Suez University, Suez, Egypt
9: Now at British University in Egypt, Cairo, Egypt
10: Also at Fayoum University, El-Fayoum, Egypt
11: Now at Helwan University, Cairo, Egypt

12: Also at Université de Haute Alsace, Mulhouse, France
13: Also at Skobeltsyn Institute of Nuclear Physics, Lomonosov Moscow State University, Moscow, Russia
14: Also at CERN, European Organization for Nuclear Research, Geneva, Switzerland
15: Also at RWTH Aachen University, III. Physikalisches Institut A, Aachen, Germany
16: Also at University of Hamburg, Hamburg, Germany
17: Also at Brandenburg University of Technology, Cottbus, Germany
18: Also at MTA-ELTE Lendület CMS Particle and Nuclear Physics Group, Eötvös Loránd University, Budapest, Hungary
19: Also at Institute of Nuclear Research ATOMKI, Debrecen, Hungary
20: Also at Institute of Physics, University of Debrecen, Debrecen, Hungary
21: Also at Indian Institute of Technology Bhubaneswar, Bhubaneswar, India
22: Also at Institute of Physics, Bhubaneswar, India
23: Also at University of Visva-Bharati, Santiniketan, India
24: Also at University of Ruhuna, Matara, Sri Lanka
25: Also at Isfahan University of Technology, Isfahan, Iran
26: Also at Yazd University, Yazd, Iran
27: Also at Plasma Physics Research Center, Science and Research Branch, Islamic Azad University, Tehran, Iran
28: Also at Università degli Studi di Siena, Siena, Italy
29: Also at INFN Sezione di Milano-Bicocca; Università di Milano-Bicocca, Milano, Italy
30: Also at Purdue University, West Lafayette, U.S.A.
31: Also at International Islamic University of Malaysia, Kuala Lumpur, Malaysia
32: Also at Malaysian Nuclear Agency, MOSTI, Kajang, Malaysia
33: Also at Consejo Nacional de Ciencia y Tecnología, Mexico city, Mexico
34: Also at Warsaw University of Technology, Institute of Electronic Systems, Warsaw, Poland
35: Also at Institute for Nuclear Research, Moscow, Russia
36: Now at National Research Nuclear University 'Moscow Engineering Physics Institute' (MEPhI), Moscow, Russia
37: Also at Institute of Nuclear Physics of the Uzbekistan Academy of Sciences, Tashkent, Uzbekistan
38: Also at St. Petersburg State Polytechnical University, St. Petersburg, Russia
39: Also at University of Florida, Gainesville, U.S.A.
40: Also at P.N. Lebedev Physical Institute, Moscow, Russia
41: Also at California Institute of Technology, Pasadena, U.S.A.
42: Also at Budker Institute of Nuclear Physics, Novosibirsk, Russia
43: Also at Faculty of Physics, University of Belgrade, Belgrade, Serbia
44: Also at University of Belgrade, Faculty of Physics and Vinca Institute of Nuclear Sciences, Belgrade, Serbia
45: Also at Scuola Normale e Sezione dell'INFN, Pisa, Italy
46: Also at National and Kapodistrian University of Athens, Athens, Greece
47: Also at Riga Technical University, Riga, Latvia
48: Also at Universität Zürich, Zurich, Switzerland
49: Also at Stefan Meyer Institute for Subatomic Physics (SMI), Vienna, Austria
50: Also at Gaziosmanpasa University, Tokat, Turkey
51: Also at Istanbul Aydin University, Istanbul, Turkey
52: Also at Mersin University, Mersin, Turkey
53: Also at Cag University, Mersin, Turkey

54: Also at Piri Reis University, Istanbul, Turkey
55: Also at Izmir Institute of Technology, Izmir, Turkey
56: Also at Necmettin Erbakan University, Konya, Turkey
57: Also at Marmara University, Istanbul, Turkey
58: Also at Kafkas University, Kars, Turkey
59: Also at Istanbul Bilgi University, Istanbul, Turkey
60: Also at Rutherford Appleton Laboratory, Didcot, United Kingdom
61: Also at School of Physics and Astronomy, University of Southampton, Southampton, United Kingdom
62: Also at Instituto de Astrofísica de Canarias, La Laguna, Spain
63: Also at Utah Valley University, Orem, U.S.A.
64: Also at Beykent University, Istanbul, Turkey
65: Also at Bingol University, Bingol, Turkey
66: Also at Erzincan University, Erzincan, Turkey
67: Also at Sinop University, Sinop, Turkey
68: Also at Mimar Sinan University, Istanbul, Istanbul, Turkey
69: Also at Texas A&M University at Qatar, Doha, Qatar
70: Also at Kyungpook National University, Daegu, Korea